# DIFFUSION TENSOR IMAGING REVEALS CORRELATIONS BETWEEN BRAIN CONNECTIVITY AND CHILDREN'S READING ABILITIES

By

Qiuyun Fan

Thesis

Submitted to the Faculty of the

Graduate school of Vanderbilt University

in partial fulfillment of the requirements

for the degree of

MASTER OF SCIENCE

in

Biomedical Engineering

May, 2011

Nashville, Tennessee

Approved by:

Professor Adam W. Anderson

Professor Laurie E. Cutting

DEDICATION

As a collaborative work, it would not be possible for me to finish this thesis without the devotion and hard work of my colleagues in the DTI group. First, I would like to express my greatest gratitude to my advisor, Prof. Adam W. Anderson, for his support during my master's study. His knowledge, experience, and his patience and encouragement to me led me through the technical difficulties. Many of the personal lessons I have learned from him will prove to be as important in my professional career as the technical ones. The three years in his group have been a highlight in my life and opened my eyes to a lot of innovations and opportunities. Thank you, Prof. Anderson! I would thank Dr. Laurie E. Cutting and Dr. Nicole G. Davis at the Education and Brain Research Laboratory (EBRL) for guiding and financially supporting me in my study. I am truly grateful to Dr. Zhaohua Ding, Dr. Ha-Kyu Jeong, Dr. Xin Hong, Dr. Ann Choe, and Ms. Yurui Gao. They have been very kind to me in both my research and personal life and took the effort to mentor me in my projects. I am also thankful to my colleagues in EBRL. Dr. Sheryl L. Rimrodt, Heather Harris, Aparna Pisupati, Laura Barquero, Lindsay M. Wilson, Erika Spangler and Julie Delheimer helped me in many of my research activities. I thank Suzanne N. Avery, Dr. Aize Cao, Dr. Francisca Serrano, and Gilma Adunas for all the helpful discussions. Last but not least, I express my deepest love to my family. My parents Wendong Fan and Li Han, and my boyfriend Lin Zhang gave me love and joy.

# ACKNOWLEDGEMENTS

TABLE OF CONTENTS

Page

Chapter

LIST OF FIGURES

# LIST OF TABLES

CHAPTER I


INTRODUCTION


**Overview**

Diffusion tensor imaging (DTI) (Basser et al., 1994) is a relatively new MR technique to study the white matter structures of the brain non-invasively. In white matter tissues, axons are normally well myelinated and aligned. Consequently, the random walk of water molecules in white matter has a preferential orientation along fiber bundles. The measured orientation preference, or anisotropy, of the molecular diffusion can provide valuable information about the micro-structural organization of white matter fiber bundles. These white matter fiber bundles, as an analogy to the highway system between the cortical regions, play an important role in transferring information and mediating cognitive functions. Recently, DTI has been used to study white matter properties as related to reading abilities (Klingberg et al., 2000; Niogi and McCandliss, 2006; Catani et al., 2005). In other studies, a topological network is constructed with the help of DTI based tractography to map the connectivity of the brain (Hagmann et al., 2008).

In this chapter, the following topics will be covered: (1) the basic principles of DTI; (2) the concepts and implications of brain connectivity; and (3) current research in regard to the relationship between reading abilities and functional or structural features of the brain, primarily focusing on studies involving imaging modalities.

# Diffusion Tensor Imaging

*Water diffusion in biological samples*

Diffusion refers to the random translational motion of particles driven by thermal energy. Biological systems are comprised of an abundance of water. Under the assumption of Brownian motion, the displacement of a particular water molecule and the time, $t$, allowed for it to diffuse can be related through Einstein's formula,

$$r = \sqrt{nDt}$$

where $r$ is the root mean square displacement, $D$ is the diffusion coefficient, and $n$ is determined by dimensionality (i.e., $n = 2$ for one dimensional scenario, 4 for two dimensional and 6 for three dimensional diffusion). In a biological sample, however, the measured diffusion coefficient is the ensemble average of all the water molecules within the voxel, so the averaged diffusivity is named apparent diffusivity, or apparent diffusion coefficient (ADC) to distinguish the measured value from the intrinsic diffusion coefficient of pure water.

*Diffusion weighted imaging*

The amount of Brownian motion during a given time period, characterized by the ADC, can be measured by diffusion weighted imaging techniques. The Pulsed Gradient Spin Echo (PGSE) experiment relates the MR signal drop to diffusion (Stejskal and Tanner, 1965) (Figure 1), where the signal intensity of the spin echo, $S$, is attenuated with respect to the baseline signal without diffusion weighting, $S_0$, via the relation,

$$\frac{S}{S_0} = e^{-bD_{app}}$$

where $D_{app}$ is the ADC, and $b = \gamma^2 G^2 \delta^2 (\Delta - \frac{\delta}{3})$ is the diffusion weighting factor, or b

factor, as a function of gyromagnetic ratio $\gamma$, the amplitude of the gradient pulse $G$, pulse

duration $\delta$, and the time interval $\Delta$ between the de-phasing and refocusing gradient pulses.
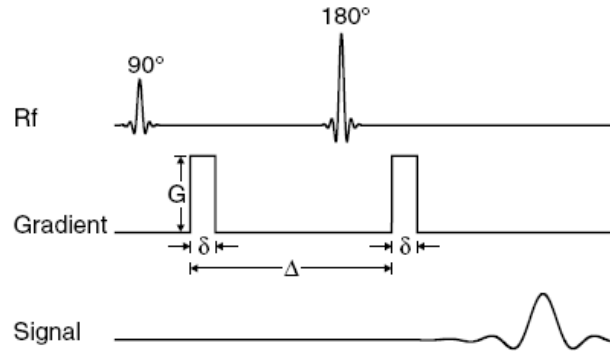


Figure 1. The PGSE paulse sequence diagram.
A pair of identical diffusion sensitizing gradient pulses is applied along a prescribed direction before and after the 180° RF pulse. Spins are phase-encoded according to their initial positions due to the first gradient pulse, and then allowed to diffuse freely for a time interval $\Delta$. After the 180° RF pulse, the second gradient pulse of the same amplitude G and duration $\delta$ is aimed to cancel the position dependent phase if the spins remain stationary during the time interval $\Delta$.

Another aspect of diffusion is directionality. In an isotropic medium, such as in the

cerebrospinal fluid (CSF) of the ventricular system (Basser and Pierpaoli, 1996), a water

molecule has an equal chance to walk along any direction. The measured ADCs are

identical when the diffusion sensitizing gradient is applied in different directions, and

thus the ADC can be obtained from two measurements, i.e., one with diffusion weighting

gradient pukes and one without. However, in other tissues like white matter fiber bundles,

where axons are wrapped with relatively impermeable myelin and are normally

coherently oriented, it exhibits higher apparent diffusivities parallel to the axons'

orientation than perpendicular to them (Moseley, et al., 1990; Pierpaoli and Basser, 1996).

The diffusion can no longer be characterized by a single scalar value of ADC, so a more complex model is needed to describe the anisotropic diffusion.

*Diffusion tensor imaging: what does it imply?*

With the assumption of Gaussian diffusion, the displacements of water molecules can be represented by a diffusion tensor (Basser et al., 1994), a 3x3 symmetric matrix, i.e.,

$$\boldsymbol{D} = \begin{bmatrix} D_{xx} & D_{xy} & D_{xz} \\ D_{xy} & D_{yy} & D_{yz} \\ D_{xz} & D_{yz} & D_{zz} \end{bmatrix}$$

where the elements on the diagonals are the apparent diffusivities along the three orthogonal axes of the (x, y, z) coordinate system, and the off diagonal elements are proportional to the covariance between molecular displacements in orthogonal directions. The eigenvalues of the tensor have physical meanings – the apparent diffusivities along the three principal axes of the diffusion tensor. The eigenvector corresponding to the largest eigenvalue $\lambda_1$ is termed the principal diffusion direction. The envelope of the tensor ellipsoid (Figure 2) depicts the isosurface of the probability density function (PDF) of a spin's molecular displacements.
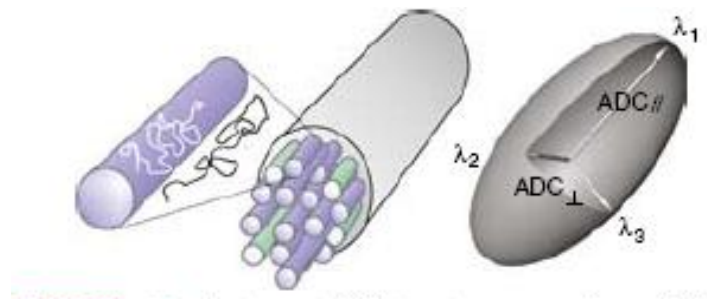


Figure 2. Ellipsoidal representation of the diffusion tensor.
The envelope of the tensor ellipsoid depicts the iso-surface of the probability density function (PDF) of a spin's molecular displacements. As predicted by Einstein's equation, the axes of the ellipsoid are scaled by the eigenvalues of the diffusion tensor.

The diffusion tensor provides important information about the microscopic composition, structure and organization of the tissue under study. Above all, fractional anisotropy (FA) (Basser and Pierpaoli, 1996; Beaulieu, 2002) is one of the most widely used scalar parameters derived from eigenvalues of a diffusion tensor to measure how much the diffusion envelope deviates from a sphere. For isotropic tissue samples, FA is close to 0, while for very anisotropic samples, the corresponding diffusion tensor will be stretched towards poles that are aligned along the fiber bundles, and the FA can approach 1. More often than not, a decreased FA is related to tissue damage or diseased status (Beaulieu et al., 1996). In addition, the principal diffusion direction is assumed to be consistent with the orientation of the underlying structure, which becomes the basis of the DTI-tractography (Mori and van Zijl, 2002; Lori et al., 2002).
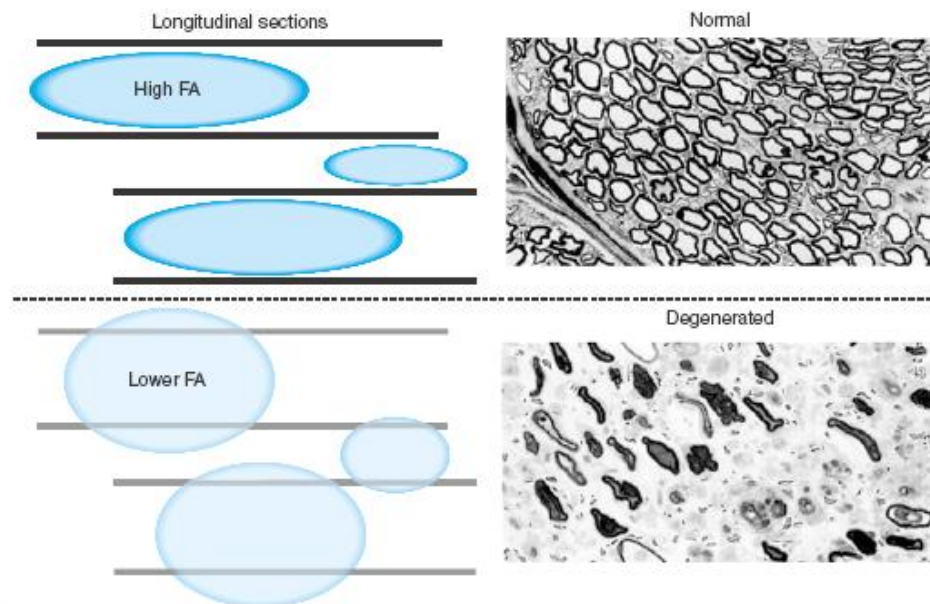


Figure 3. Illustration of FA indicative of structural damage.
On the left is the cartoon illustration of reduced anisotropy due to damage in axons and myelin that result in a loss of directional barriers to water diffusion. On the right, electron micrographs are adapted from normal and degenerated frog sciatic nerve (Beaulieu et al., 1996).

**Brain Connectivity**

The human brain is a complex biological network. How the processing elements are interconnected makes individual brains distinct from each other. Brain connectivity is used to describe the intrinsic linkage between neuronal units that are remotely distributed. Functional connectivity, effective connectivity, structural connectivity, etc., reflect different aspects of the linkage. For structural connectivity, postmortem examinations can be carried out in ex-vivo samples, bio-tracers and imaging contrast agents can be used for in-vivo studies, DTI techniques are non-invasive alternatives to reconstruct the macroscopic pattern of tissue structures, and optical imaging methods are also emerging in this field. This work focuses on the structural connectivity obtained from DTI based tractography and how it is related to the functions it supports.

*Tractography*

Tractography is the process of integrating voxelwise fiber orientations into a pathway that connects remote brain regions. It relies on the fundamental assumption that the water diffusion is least restricted along the axes of axons, if the neural fibers are coherently aligned along a common axis. Tractography algorithms can be local or global, deterministic or probabilistic, model based or model free; they can rely on simple (Mori et al., 1999) or complex (Parker and Alexander, 2003, 2007) representations of diffusion in white matter. This section briefly reviews DTI based fiber tracking techniques involved in this study, including streamline tractography (Mori et al., 1999) and probabilistic tractography.

The most intuitive and commonly used fiber tracking technique is streamline tractography. From the previous sections we know that on the voxel level, a principal diffusion direction can be estimated by DTI, which is assumed to be collinear with the neuronal fiber bundle axis. By starting at a proper seed point (i.e., in the middle of a well organized fiber bundle), a streamline representation of the bundle can be reconstructed by following the local vector information on a step-by-step basis. Since fiber tracking is an integration process, the reconstruction accuracy is very susceptible to errors in local vector estimates. To limit false positives, the algorithm is stopped when the front of the streamline steps into a local area where the directional uncertainty is above a preset threshold. This directional uncertainty corresponds to hypo-intensity in FA maps, which may be due to various reasons such as low SNR, partial volume effects at boundaries of white matter and gray matter or at the intersection of multiple fiber bundles, etc. Another criterion for a streamline to stop is high, because it is assumed that no sharp turns exist in deep white matter. The employment of spatial interpolation (Mori et al., 1999; Lazar and Alexander, 2003; Pajevic et al., 2002) can overcome, to some degree, the effects of noise in the local orientation estimates and improve the smoothness of reconstructed fiber tracts, but a simple streamline algorithm is still very vulnerable to error accumulation due to its deterministic nature. Probabilistic algorithms have recently been proposed to track through regions with high uncertainty. These will be discussed in later sections.

*Implications of brain connectivity*

Structural connectivity describes a physical network of connections, which correspond to fiber pathways or individual synapses.  DTI techniques cannot identify cellular synapses,

but they provide probabilistic macroscopic connection profiles which are non-invasive in-vivo estimates of structural connectivity.

From the connectivity point of view, cortical regions of the brain and thed fiber pathways connecting them can be conceptualized as nodes and edges of a network. The nodes perform various executive functions, and the edges serve as the highway for information transfer and mediate complex cognitive functions that require collaboration of multiple executive functions. The territory of a node can be determined by anatomical landmarks (Hagmann et al., 2007), the sites of activation in fMRI tasks, or cross-correlations between structure and function (Johansen-Berg et al., 2004). Depending on the specific purpose of the study, the edge can either be binary, representing existence or not, or carry a weight on them, such as distance or fiber density (Honey et al., 2007; Sporns et al., 2007; Hagmann et al., 2008).

Whether and how structural connectivity is related to brain function is a key question in the brain connectivity analysis. The results of Hagmann et al. (2008) (Figure 4) suggested that direct linkage by strong fiber pathways may be predictive of significant functional connections as well, while conversely, strong functional relations may also exist between structurally non-connected regions that are interacting via indirect pathways. Other studies provided supporting evidence that relates individual structural connectivity patterns to functional connectivity which may account for behavioral variations (Boorman et al., 2007). How structural connections determine functional connections was demonstrated by observations of functional connectivity in the brain of a patient before and after undergoing neurosurgery (Johnston et al., 2008). For a review of the various ways in which structural and functional connectivity are combined, see Rykhlevskaia et

al. (2008). Given these clues, it's likely that a link between structural connectivity and brain function, however the detailed relations are still open for exploration.
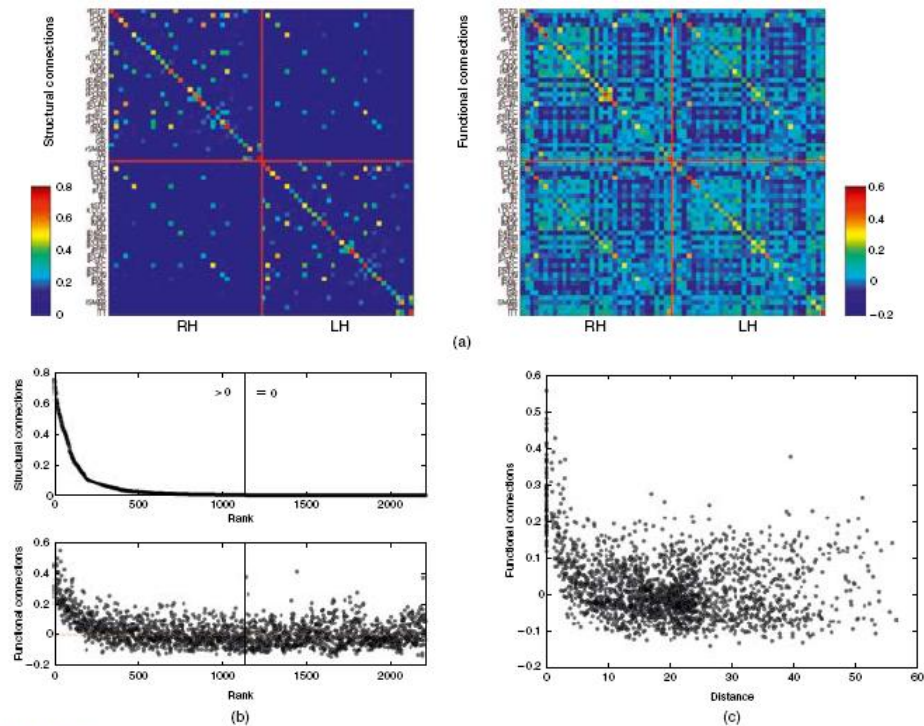


Figure 4. Whole-brain comparison of structural and functional connectivity. (a) Matrix of structural connections as estimated by diffusion imaging (left) and functional connections as estimated from resting state fMRI (right), averaged over the same group of five participants. Network nodes correspond to 66 anatomical regions. (b) Rank-ordered distribution of structural connections (top) and comparison to functional connections displayed in the same order (bottom). Note that some strong functional connections exist in places where no corresponding structural connections are detected. (c) Scatter plot of the distance between all pairs of nodes and the strengths of their functional connections. Connections with a distance of zero represent intra-regional correlations on the main diagonal of the functional connectivity matrix shown in (a). Note the prevalence of strong functional connections between nodes that are topologically close. Distance is computed from the weighted structural connection matrix. (Hagmann et al., 2008)

Given the knowledge that cortical regions are the primary sites of cognitive functions, the ability to extract cortico-cortical connection patterns is an important aspect of brain connectivity studies. One approach toward this goal is to explore gray matter thickness

correlations (He et al. 2007; Chen et al., 2008). While these studies map the entire human cortex and the data are highly consistent with previous findings, the method suffers from a few shortcomings such as less straightforward interpretation of connection patterns and the requirement of huge sample sizes. As will be discussed below, the work of this thesis takes advantage of the ability of probabilistic tractography to penetrate the white/gray matter boundaries, and thus is able to extract cortico-cortical connections specific to regions that are responsible for particular brain functions.

## Current Opinions in Reading and the Brain

Cognitive tasks like reading need a set of distributed cortical areas that work together toward accomplishing a desired goal. Each neural unit has its own contribution; activation is synchronized across participating areas. In regard to reading ability, the neural network can be generally associated with neuroanatomical areas within the left perisylvian region. However, areas within this region have their own cognitive specialization and vary in their importance to reading ability (Shaywitz et al., 2004).

*Cortical regions important to reading*

Before neural imaging modalities such as PET and fMRI become widely utilized in studies of brain function, the knowledge on specific functions of an anatomical region is mostly gained from clinical cases where brain damage and functional deficits are consistently observed simultaneously. In terms of reading abilities, an abundant functional neuroimaging literature links individual variability in word recognition skills to variations in the neuronal functioning of three anatomical areas within the Perisylvian

network: occipito-temporal cortex (OTC), temporo-parietal cortex (TPC), and inferior frontal gyrus (IFG). Quite a few studies have consistently reported that in individuals with reading disability (RD), decreased activity was observed in the left OTC (Brunswick et al., 1999; Paulesu et al., 2001) and left TPC (Rumsey et al., 1997; Horwitz et al., 1998; Brunswick et al., 1999), while increased activity was observed in right TPC (Shaywitz and Shaywitz, 2003) region. However, children with RD who respond to reading intervention exhibit significantly increased activation of left hemisphere TPC and decreased activation of right hemisphere TPC as compared to pre-intervention profiles (Simos et al., 2002, 2006; Aylward et al., 2003; Shaywitz et al., 2004), indicating plasticity in the functional pattern across participating cortical regions.

*The role of white matter in reading behavior*

Reading is a complex cognitive behavior, which requires the collaboration of different cortical regions. As a string of letters appears in the retina, the visual cortex in the occipital lobe is activated (Puce et al., 1996; Dehaene et al., 2002). The letterbox in the brain located in the occipital-temporal regions recognizes the pattern as related to language. The phonological processing centers quickly decode the letters into phonemes (Rumsey et al., 1997; Nittrouer, 1999; Temple et al., 2001), and probably at the same time the meaning of the word is recalled which is thought to involve inferior frontal regions (Mesulam, 1990; Perry et al., 2007). Normally, it takes approximately one fifth of a second for brains to finish the whole process and recognize a word (Tarkiainen et al., 2002). Given that reading relies so much on efficient and accurate information transfer

between cortical regions, how white matter properties affect reading performance becomes a key question in reading studies.

Current research supports the hypothesis that white matter structure variations in individuals are behaviorally relevant and that they can be studied in vivo with diffusion MRI. In fact, differences in white matter have been shown in several studies comparing children with reading difficulty to normal readers (Klingberg et al., 2000; Beaulieu et al., 2005; Deutsch et al., 2005; Niogi and McCandliss, 2006), where significant differences in white matter integrity were reported in temporal-parietal regions. Lower FA in the left corona radiata is consistently reported, and was considered to be relevant to poor reading performance. Although a precise prediction of functional and behavioral consequences that result from white matter changes is still hard to make, more and more evidence suggests that white matter properties such as myelination, packing density, and fiber coherence might affect behavior by modulating information transfer across the brain network. Specific to reading, how strongly the cortical regions within the Perisylvian territories are connected to each other appears to be associated with reading ability.

## Goal of This Study

As learned from previous sections, by measuring the spatial distribution of response in cortical regions to stimuli, functional brain activity studies can map cortical involvement in tasks, but are insufficient to identify the physical mechanisms that underlie variance in the level of involvement, i.e., whether reduced activation is due to retarded cortical units or due to impaired synchronization among them. On the other hand, comparisons of local properties identify differences in white matter structures between good and poor readers,

which is suggestive of a communication problem. However, standing in the middle of the brain, it's difficult to tell how the difference at that focal site contributes to behavioral differences as related to communication efficiency across many cortical units that are interconnected to each other. The brain functions like a network, each node of which plays a unique role and information is exchanged through the edges connecting them. Which connection in the network becomes the limiting factor of information transfer and finally leads to behavioral deficits is not clear. The goal of this work is to study the relationship between brain connectivity and responsiveness to intervention (RTI, as a measure of children's reading abilities) (IDEA, 2004), and explore whether a correlation exists between brain structural connectivity and RTI performance.

CHAPTER II


METHOD


Participants for this study were recruited from first graders. The participants were screened for handedness, IQ, brain injuries, and other physical disabilities. Reading intervention was administered based on their performance in the classroom. Information on each participant's reading skills was obtained throughout the intervention process and structural MRI and DTI scans were acquired at the end of the intervention. High resolution structural MR images were then used to identify anatomical regions. A connectivity analysis focused on cortical and sub-cortical regions of interest (ROI) that were identified in previous studies as related to reading skills. Probabilistic tractography was performed between pairs of ROIs to calculate the connectivity strength between brain regions. The outcome from connectivity analysis was correlated with participant's reading scores to explore the relationship between white matter properties and reading abilities.


### Participants and Behavioral Measures

The variation in reading skills is due to a combined effect of variations in brain architecture, education and environment. As age increases, the experience of reading drives the brain to form compensatory mechanisms to offset the deficits, if any, in brain function that are normally employed in reading. This will possibly lead to a complicated situation, where the physical variation exists in the brains, but the behavioral variation

does not in reading performance – plasticity of the brain shadows it. This may raise difficulties in identifying anatomical features that are characteristic of specific skills. Hence, abnormality in children's reading ability as related to brain features is of particular interest, since the gaining of reading experience is just started and the diverse complementary approaches throughout the population may not yet dominate individual differences in brain structure.

*Recruitment and grouping criteria*

Fifteen first graders (mean age ± STD = 7.5 ± .43 year old) were recruited for this study. The participants were from a sample of children in Nashville participating in a federally funded randomized control trial (RCT). The RCT explores the effectiveness of response to intervention (RTI) as a means of identifying and preventing RD. All participants, including control participants, were screened and determined to be at-risk for reading difficulties at the beginning of first grade. Children with brain injury, other physical disabilities, severe emotional problems, uncorrected sensory disorders, ADHD, or an IQ < 80 were excluded during recruitment for this neuroimaging portion of the project. No child had limited proficiency in English. No restriction was made for gender, ethnicity, or socioeconomic status. This study was approved by the Vanderbilt University Institutional Review Board. Written informed consent was obtained from the children's guardians. Written assent was obtained from the children.

Of the fifteen datasets, four were not included due to severe head motion in the neuroimaging session that rendered the tractography data unreliable. The remaining 11 participants were placed into groups based upon RCT categorization (described in

Behavioral Measures and Responsiveness section, below). As such, classroom controls (CNT; n=5) were defined as children who were initially identified as at risk in the fall of first grade but benefited from classroom-based tier 1 instruction and therefore did not qualify for small-group tier 2 reading intervention. Treatment responders (R; n=2) were defined as children who did not benefit from tier 1 instruction, were eligible for small-group tier 2 reading intervention, and achieved adequate results on behavioral measures indicating response to intervention. Treatment non-responders (NR; n=4) were children who did not benefit from tier 1 instruction, were eligible for small-group tier 2 reading intervention, and did not achieve adequate results on behavioral measures, indicating a failure to respond to intervention.

*Behavioral measures and responsiveness*

Within the RCT, children's response to the instruction was estimated with a measure of word identification fluency (WIF; Compton et al., 2010; Fuchs et al., 2004), which was administered weekly. Growth modeling of WIF over six weeks at the beginning of the school year indicated each child's responsiveness to the general classroom instruction (prior to small-group tier 2 intervention). Children identified as unresponsive to general classroom instruction were assigned to small-group tier 2 intervention (tier 2), in which trained research assistants provided a prescribed reading intervention three days per week for 17 weeks. For participants receiving tier 2 intervention, weekly progress monitoring using WIF continued throughout the course of intervention. Upon conclusion of the intervention, responsiveness was determined using WIF intercept and slope over the duration of the intervention. It is important to note that for the imaging study, limitations

in sample size necessitated ranking participants by WIF intercept and slope and dividing participants to designate equal groups of responders and non-responders. These designations of responders and non-responders were used in all subsequent analyses.

Pre and post test behavioral measures were administered to all participants receiving tier 2 intervention. As stated above, the WIF growth was used to identify the participants' group membership. The pre- and post test measures listed below were correlated with imaging data.

- *Word Identification Fluency* (WIF). WIF consists of single-page lists of 100 high-frequency words randomly sampled from the Dolch pre-primer, primer, and first-grade level lists (Fuchs et al., 2004). The task is to read as many words as possible in 1 min.

- *Untimed word identification skill*. The Woodcock Reading Mastery Test – R/NU: Word Identification (WRMT-R: WID, Woodcock, 1998) is a norm-referenced test in which subjects read individual words ordered in difficulty until six sequential incorrect responses occur.

- *Untimed decoding skill*. The Woodcock Reading Mastery Test – R/NU: Word Attack (WRMT-R: WAT, Woodcock, 1998) is a norm-referenced test that requires subjects to pronounce decodable pseudowords presented in ordered difficulty until a ceiling of six sequential incorrect responses is reached.

- *Sight word reading efficiency*. The Test of Sight Word Reading Efficiency (TOWRE: SWE, Torgesen et al., 1997) is a norm-referenced measure of sight word reading accuracy and fluency in which participants read a list of words of increasing difficulty for 45 sec.

- *Phonemic decoding efficiency*. The Test of Phonemic Decoding Efficiency (TOWRE: PDE, Torgesen et al., 1997) is a norm-referenced measure of decoding accuracy and fluency that requires participants to read a list of decodable pseudowords of increasing difficulty for 45 sec.

As part of the intake procedure, letters were sent to the parents of children who had successfully completed the RCT research protocol (including R, NR, and C participants) and met our recruitment criteria. All participants attended a single imaging session, in which each child was acclimated to the lab and received a child-oriented explanation of the study procedures. A play tunnel and a mock scanner were used to practice the tasks and prepare the child for the scanning environment.

## Imaging Data Acquisition and Image Processing

On the imaging side, both high resolution anatomical images and diffusion weighted images were acquired for each participant. The imaging data were passed through a processing pipeline (Figure 5). The first step was brain parcellation using T1-weighted images. For the diffusion weighted images, eddy current artifacts were corrected by linearly registering the diffusion weighted images to the non-diffusion weighted image. After EPI distortion correction using field maps, T1-weigted images and diffusion weighted images were co-registered, and the ROI masks obtained in T1 space were aligned in DTI space to get ready for fiber tracking.
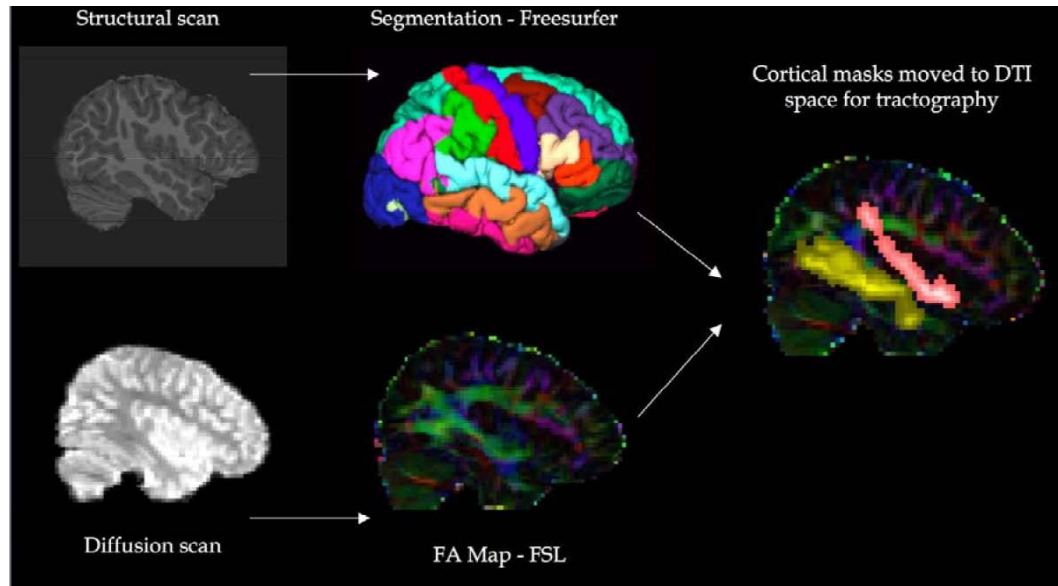
Figure 5. Image processing pipeline.
Diffusion weighted images were corrected for image distortions due to both eddy current and EPI artifacts, the latter using the acquired field maps and FSL software. Cortical reconstruction and volumetric segmentation were performed with the Freesurfer image analysis suite to identify the cortical and subcortical gray matter regions of interest on the T1-weighted structural scan. Then T1-weighted images were aligned with diffusion weighted images to prepare for the fiber tracking in future steps.

*Data acquisition*

All imaging was performed on a research-dedicated Philips Achieva 3T MR scanner.

1. Structural imaging

High resolution 3D T1-weighted anatomical images were acquired (in a sagittal orientation) in just under 6 min. This was an inversion-prepared turbo field echo sequence (IR-TFE) with TI=916ms, TR=7.9ms, TE=3.6ms, SENSE acceleration factor of 2, matrix size 256x256x170, and FOV 170x256x256 mm$^3$ for isotropic 1mm resolution. These images were used for subsequent scan prescription and for cortical parcellation.

2. Diffusion weighted imaging

To measure brain tissue microstructure, we acquired high angular resolution diffusion images using a pulsed-gradient spin echo, echo planar imaging (single shot EPI) pulse sequence to image the entire brain at 2.5 mm isotropic resolution (50 slices, 96x96 matrix, TE = 65 ms, TR = 8.5 s, SENSE acceleration factor 2). We acquired 10 non-diffusion weighted and 92 diffusion weighted image volumes (92 directions at b=1600 s/mm$^2$).

3. Field map

To correct for EPI distortions, we acquired a field map (1.875 x 1.875 x 4.934 mm voxels, TE = 2.9 and 3.9 ms, TR = 173 ms, scan time 28 s), with a magnitude volume and a phase accumulation volume.

*DTI artifacts correction*

1. Eddy current correction

Eddy currents are the electric currents induced in conducting surfaces near the gradient coils by a changing magnetic field. Eddy currents can cause artifacts in diffusion weighted images such as stretching and shearing, which can mostly be corrected in post-processing by affine registration (Netsch and van Muiswinkel, 2004). The eddy current influence on gradient fields becomes more significant farther from the center of the magnet, and thus the worst distortion occurs at the outer border of the brain. In brain FA maps, FA values will normally range from 0 to 1. However in the presence of eddy current artifacts, one or more of the eigenvalues derived from the diffusion tensor can be negative as a result of the misalignment of the images corresponding to different diffusion weighting gradients, and consequently the FA value can be greater than 1. Usually the eddy current artifacts will appear as a ring of hyper-intense voxels on the

border of the brain in FA maps (Figure 6). We can count the number of voxels exceeding the physically reasonable range of FA values (0 to 1) and use it to compare the performance of different affine registration tools in eddy current correction.
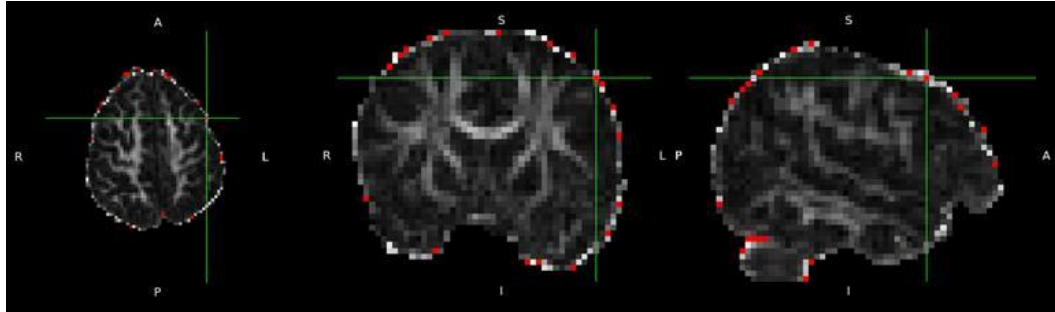


Figure 6. Eddy current artifacts as shown in gray scale FA maps.
From left to right are axial, coronal and sagittal views of a typical FA map with eddy current artifacts. The red dots label the voxels where the FA value is greater than 1. At the border of the brain, the diffusion anisotropy should not have been high. The hyper-intensity in the border voxels is due to misalignment of the diffusion weighted images corresponding to different diffusion weighting gradients.

A few software tools are available for affine registration, including the FMRIB's diffusion toolbox (FDT) (Jenkinson and Smith, 2001) provided by FMRIB's software library (FSL) (Smith et al., 2004; Woolrich et al., 2009), the slice by slice affine registration tool in the in-house Matlab scripts package (vuTools) prepared by the Vanderbilt University Institute of Imaging Science, and the affine registration tool in the Philips Research Imaging Development Environment (PRIDE). In the present study, the performance of these tools was compared (see result section), and PRIDE was finally selected for the image processing pipeline.

2. EPI distortion correction using field maps

Different tissues have different magnetic susceptibilities when placed in the magnet. Tissues with dissimilar susceptibilities, such as air-bone or air-tissue interfaces in the

sinuses, interact differently with the local magnetic fields, and lead to inhomogeneities in the magnetic field. The EPI sequence is sensitive to such field inhomogeneities, and thus DTI data acquired using EPI sequences can be distorted, especially in the inferior frontal and temporal regions. However, the inhomogeneous magnetic field can be measured. With the information in a field map, the geometric distortion and signal loss can be calculated, and then used to compensate for EPI distortion artifacts (Jezzard and Balaban, 1995).

The field map is 3D-unwrapped using a Phase Region Expanding Labeler for Unwrapping Discrete Estimates (PRELUDE) in FSL before it is used for EPI unwarping (Jenkinson, 2003). The EPI distortion correction is carried out using FMRIB's Utility for Geometrically Unwarping EPIs (FUGUE) in FSL (Jenkinson, 2001, 2004). In general, the processing starts from calculating forward EPI warps using the field map, based on the assumption that the field maps (both anatomic and real field maps) are not susceptible to the EPI sequence distortion. The calculated (forward) warps are applied to the anatomic image in the field map, before the non-diffusion weighted image is registered to it. The transformation is then inverted to convert the EPI unwarping map from field map space to DTI space. Finally, this unwarping map is applied to diffusion weighted images to correct for non-linear EPI distortions.

*Brain parcellation using structural images*

Whole brain cortical parcellation is done under the framework of FreeSurfer (Fischl, 2002, 2004), using high resolution T1-weighted MR images. The process starts from motion correction through an affine transformation with 12 degrees of freedom to the

Talairach coordinate system, followed by non-uniform intensity normalization to correct for spatial intensity inhomogeneity (Sled et al., 1998). The skull was stripped from the image (Segonne et al., 2004), and the mean intensity of the remaining brain image volume was normalized to match the atlas intensity scale built in FreeSurfer. Then the atlas brain is nonlinearly warped to each participant's brain for the atlas-based tissue segmentation, which labels the brain volume in the individual space with subcortical structures, brain stem, cerebellum, and cerebral cortex. The next step in FreeSurfer is to generate topologically correct cortical surface mapping for each hemisphere. The cortical surface is the tissue interface between white matter and gray matter or between gray matter and CSF. For each hemisphere in the brain, the gyri and sulci are unfolded, inflated to the surface of a unit hemisphere, and projected to a standard spherical coordinate system. The surface inflation conforms to minimal metric distortion. The parcellation process also takes the steps of topology correction (Fischl et al., 2001; Segonne et al., 2007) and surface based warping to align anatomically homologous points. The result is a complete labeling of cortical sulci and gyri. The surface mapping is then extended to gray matter volume parcellation, resulting in segmented regional cortical volumes.

*Registration between anatomical and diffusion weighted images*

The anatomical regions identified in T1 space need to be transformed into DTI space to prepare for tractography. Since a previous step has corrected for the nonlinear EPI distortion in diffusion weighted images, the alignment between diffusion weighted and T1-weighted images is carried out using FMRIB's linear image registration tool (FLIRT)

(Jenkinson and Smith, 2001). The first step is to register the lower resolution non-diffusion weighted image in the DTI scan to the higher resolution T1-weighted image with 12 degrees of freedom and trilinear interpolation. As the registration is inter-modal, the normalized mutual information is selected as the cost function. The transformation is then inverted and applied to the cortical labeling in T1 space. In order to preserve the regional volumes, trilinear interpolation is dropped and voxels located at regional boundaries are assigned to their nearest neighbors. At this point, every voxel in the diffusion weighted image volume has a label that corresponds to a specific anatomical region.

## Structural Brain Connectivity

Structural connectivity measurements aim to reveal the physical connections that underlie the communications between cortical neuronal units. With the help of DTI techniques, deterministic streamline tractography has been used to quantify structural connectivity (Hagmann et al., 2007), but harsh stopping criteria are used in deterministic streamline algorithms to avoid false positives, which render low sensitivity in detecting fibers penetrating though white/gray matter boundaries. The connectivity index employed in this work is calculated under the framework of probabilistic tractography, which is able to track through low FA locations and provides the possibility to map cortico-cortical connections that originate from and enter gray matter.

*Regions of interest*

To investigate the relationship between WM connectivity and responsiveness to instruction, we selected nine cortical ROIs that have strong theoretical justification for playing a part in reading skill (Table 1). Each region is involved in several different behavioral processes; we list in Table 1 only the behaviors of interest to the current study. This study will focus on these regions, and the connectivity strength will be calculated pair-wise manner among them.

**Table 1. Regions of interest**

| Anatomical Name | Acronym | Behavior of interest |
|---|---|---|
| Angular Gyrus | ANG | active during numerous verbal and written tasks |
| Fusiform | FUS | related to the automatic recognition of written words |
| Inferior Frontal Sulcus | IFS | active during naming tasks |
| Insular Cortex | INS | supports phonological processing, particularly sublexical spelling to sound translation |
| Pars Opercularis | OPE | subregion of Broca's Area mainly related to phonological processing but also syntactic processing |
| Planum Temporale | PLA | integration of orthographic with phonological and lexical features of printed words |
| Superior Temporal Cortex | STC | associated with linking letters to corresponding phonemes |
| Thalamus | THA | related to reading words out of context |
| Pars Triangularis | TRI | subregion of Broca's Area mainly related to syntactic but also semantic and phonological processing |

*Probabilistic fiber tracking*

1. Local diffusion parameters estimation

The local diffusion parameters are estimated using the BEDPOSTX (Bayesian Estimation of Diffusion Parameters Obtained using Sampling Techniques allowing for crossing fibers) (Behrens et al., 2003a, 2007) tool implemented in FSL. Instead of modeling crossing fibers directly, BEDPOSTX employs a Bayesian method called automatic relevance determination (ARD), so that multiple directions are resolved where and only where they are supported by the data. The ARD process starts from a complex model with a prior initialization of the diffusion parameters, such as volume fractions and fiber orientations, and then runs Metropolis Hastings Markov Chain Monte Carlo (MCMC) to sample the diffusion parameters at each voxel. If the prediction resulting from the diffusion parameter sample is supported by actual data, it has a positive weight for this particular set of parameters and will contribute to the posterior distribution; otherwise, it is unlikely that this set of parameters are representative of the real structures we are trying to probe, and thus ARD will force it to zero. The result is that, for each parameter, the posterior likelihood distribution will have at least one peak at zero (reflecting the probability of the simpler model), and other peak(s), if any, at other relatively probable value(s) (reflecting the probability of the corresponding complex model). Given the posterior probability distribution on every parameter in the model, including the orientation and volume fractions from each fiber population, a local estimate can be obtained by sampling from the distribution.

2. Probabilistic tractography

Probabilistic tracking (probtrackx) repetitively samples from the distributions of voxel-wise principal diffusion directions, each time computing a streamline through these sampled local estimates to generate a sample of the true streamlines. By taking many such samples, the posterior distribution of the streamline or the connectivity distribution at the location can be built up. The pattern of the streamline distribution carries integrity information of the territories involved, for high directional uncertainty will cause the streamlines to disperse faster. In this case, the distribution is thus broad and consequently the probability for streamlines to pass coherently beyond this region decrease. Conversely, the streamline distribution due to well organized fiber bundles will show a more congruent and compact pattern.

For this work, the goal is to explore the cortico-cortical connections by taking advantage of probabilistic tractography's robustness in surviving high uncertainty locations such as gray matter white matter boundaries. The seed masks are specified as one of the 18 ROIs (both right and left hemispheres) as mentioned in the parcellation section. For each individual fiber tracking task, one of the other 17 ROIs serves as a termination mask. In the mean time, whiter matter is used as a waypoint mask and the thalamus is used as an exclusion mask. In other words, any of the surviving fibers would satisfy the following conditions: (1) it originates from one of the voxels within the seed region, and reaches the termination region; (2) it travels through at least one voxel of the white matter region; (3) it does not touch any of the voxels within the thalamus region, and thus indirect connection through the relay station of the thalamus is excluded from the analysis.

*The connectivity matrix*

For each pairing of seed and target regions in the fiber tracking step, the number of connecting streamlines was counted. The number of streamlines from seed $ROI_i$ to target $ROI_j$, divided by the number of voxels in the seed region, was used to quantify the one-way connection ratio, $r(i, j)$. The connectivity, or connection strength, between regions $ROI_i$ and $ROI_j$ was defined as the symmetrized connection ratio,

$$C_{sym}(i, j) = (r(i, j) + r(j, i))/2$$

Notice that, the connectivity defined in this way is the weighted average of number of connecting streamlines found forward and backward, and the weighting is the inverse of the seed region volume.

## Correlation between Behavior and Brain Connectivity

We hypothesized that we would replicate previous findings of differences in WM related to reading skill. In addition, we anticipated that children's responsiveness to reading intervention would provide additional information. To test the hypothesis, multiple linear regression was performed between connectivity indices and standardized test scores of reading proficiency to explore if a correlation exists. For each element in the connectivity matrix, among the connectivity values across participants, an individual value that deviated from the original sample mean by two standard deviations or more was defined as an outlier and removed from the associated correlation analysis. Given that the regional volumes vary across participants, we also calculated the correlation between region volume and the different behavioral measures. In addition, we also investigated age and gender influences on the behavioral and imaging results.

CHAPTER III


RESULTS


Results of both image processing steps and correlation analysis are presented below.


**Image Processing**


*DTI artifacts correction*

1. Eddy current correction

Diffusion weighted images were registered to the non-diffusion image to correct for stretching and shearing. The performance of the linear registration tool in FSL, affine registration tool in the vuTools package and the affine registration tool in PRIDE are compared in terms of number of FA values falling outside the physically reasonable range. A histogram of FA values after eddy current correction (ECC) using each tool was constructed (Figure 7). Fractional anisotropy greater than 1 is considered to be due to imperfect artifact correction. The histograms show that the affine registration tool implemented in PRIDE gives the best performance in terms of total number of FA values falling outside the physically reasonable range.
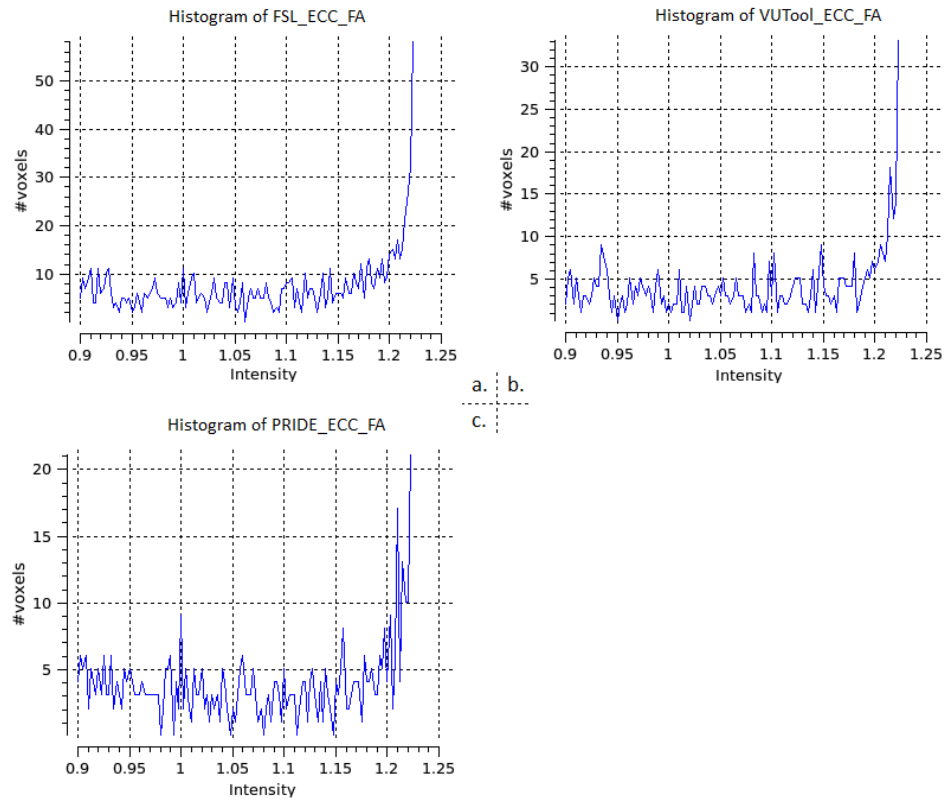
Figure 7. Comparison of eddy current correction using different tools.
The number of FA values falling outside the physically reasonable range is a reflection of misalignment between image volumes, and hence was used to compare the performance in eddy current correction of different tools, including the FDT tool in FSL (a), the in-house built Matlab scripts in the vuTools package (b), and the affine registration tool in PRIDE (c). The histogram shows that PRIDE gives the best performance in eddy current correction in terms of the number of FA values greater than 1.

30

2. EPI distortion correction using field maps

The field map is 3D-unwrapped using Phase Region Expanding Labeler for Unwrapping discrete estimates (PRELUDE) in FSL (Figure 8). A binary mask of the brain is created using the magnitude image and is then used to mask off the background of the phase map. Notice the discontinuity in the skull (white arrow) due to phase wrapping is filled up after unwrapping.
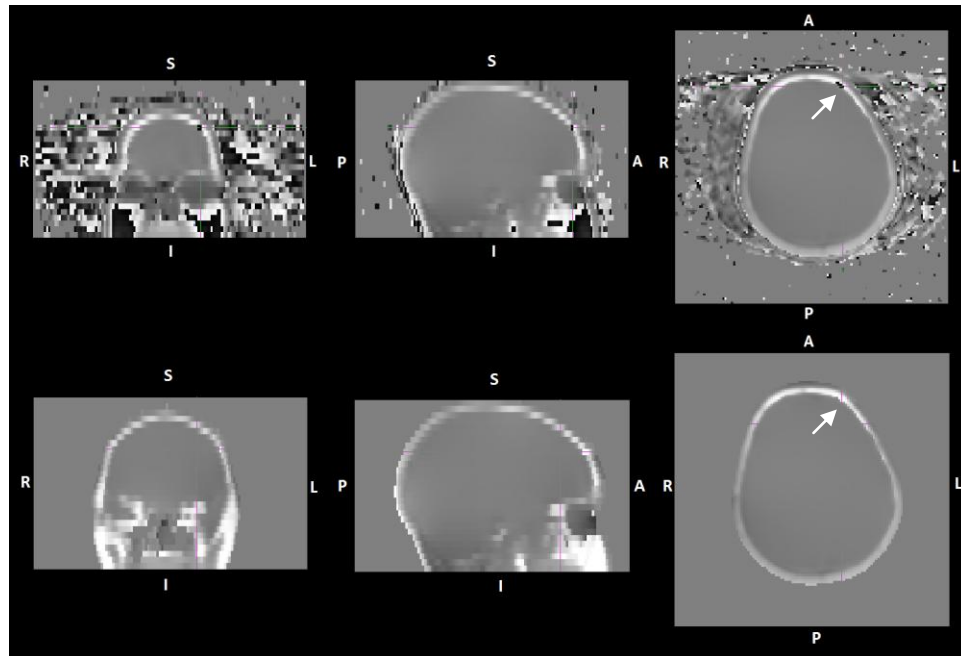


Figure 8. Phase map unwrapping.
The discontinuities in the original phase map (upper panel) are due to phase wrapping. A binary mask of the brain is created using the magnitude image and is then used to mask off the background of the phase map. Notice that using PRELUDE, the discontinuity in the skull due to phase wrapping is evened out after unwrapping (lower panel).

The result of EPI distortion correction using a field map is shown in Figure 9. The top row is the field map which is free of EPI distortion; the middle and bottom rows are the distorted DTI images, respectively. Notice the distortion in posterior brain is corrected after unwarping according to the field map.
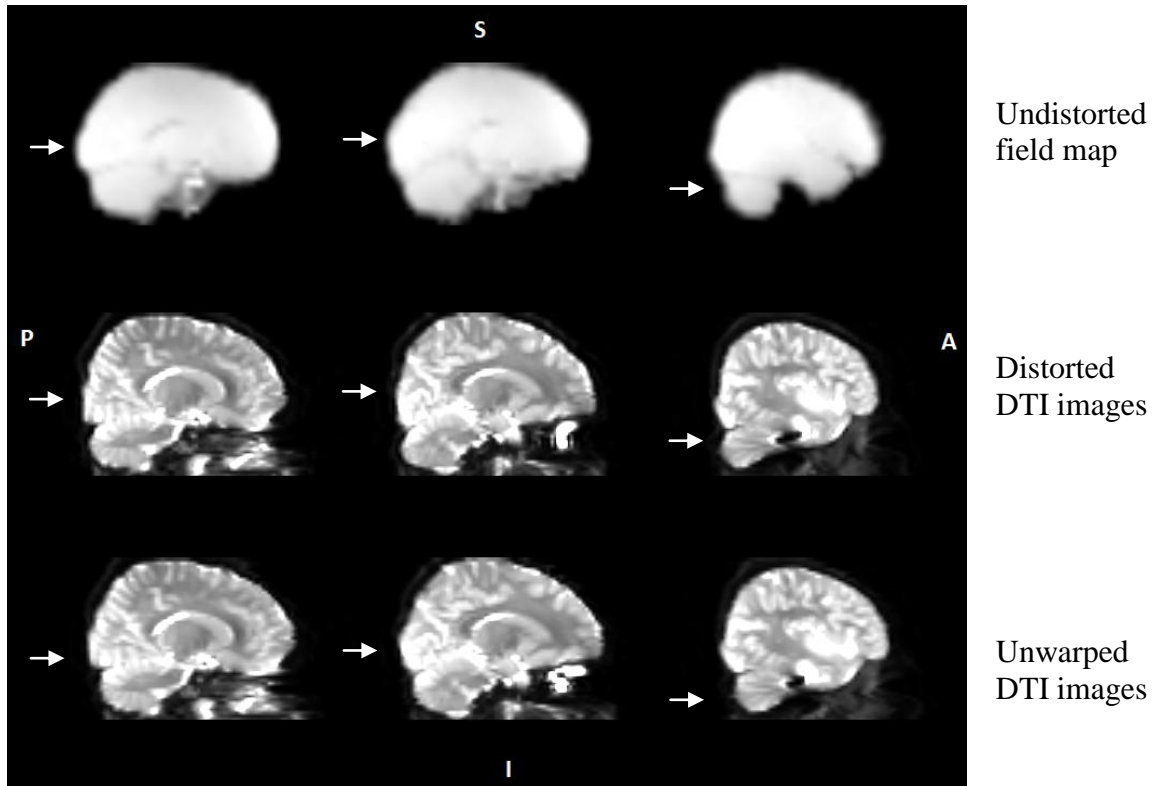


Figure 9. EPI distortion correction using a field map.
The top row is the field map without EPI distortion; the middle and bottom rows are DTI images collected using the EPI sequence. The distortions in the posterior regions are corrected by nonlinear warping. Notice the distortion in the posterior brain is recovered after unwarping according to the field map.

*Brain parcellation using structural images*

Cortical parcellation is done in FreeSurfer. This uses an atlas-based cortical surface mapping, which requires non-linear registration. It takes approximately 24 hours to process an individual participant, and Figure 10 shows a typical set of parcellation results in a participant. Each color depicted on the reconstructed surface of the brain represents a specific anatomical region.
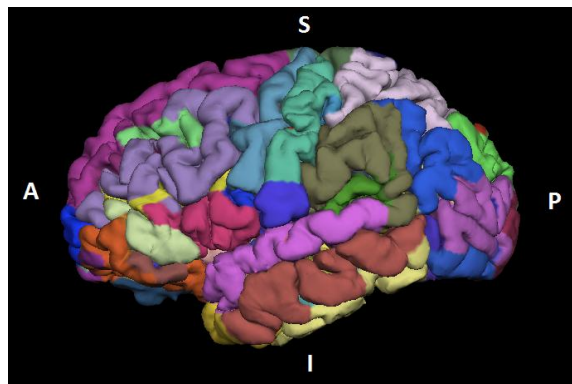


Figure 10. Cortical parcellation results from FreeSurfer.
The left hemisphere of the parcellation for a typical participant is shown. Each color depicted on the reconstructed surface of the brain represents a specific anatomical region.

## Connectivity Matrices

*Regions of interest*

As described in the methods section, nine regions in each hemisphere of the brain are selected as ROI for this study. Shown in figure 11 is how these regions are distributed in the brain. Eighteen ROIs identified in this paper are labeled in the following manner: a

prefix for cerebral hemisphere (L = left hemisphere, R = right hemisphere), a dot

following the prefix, and the acronym of an anatomical region.
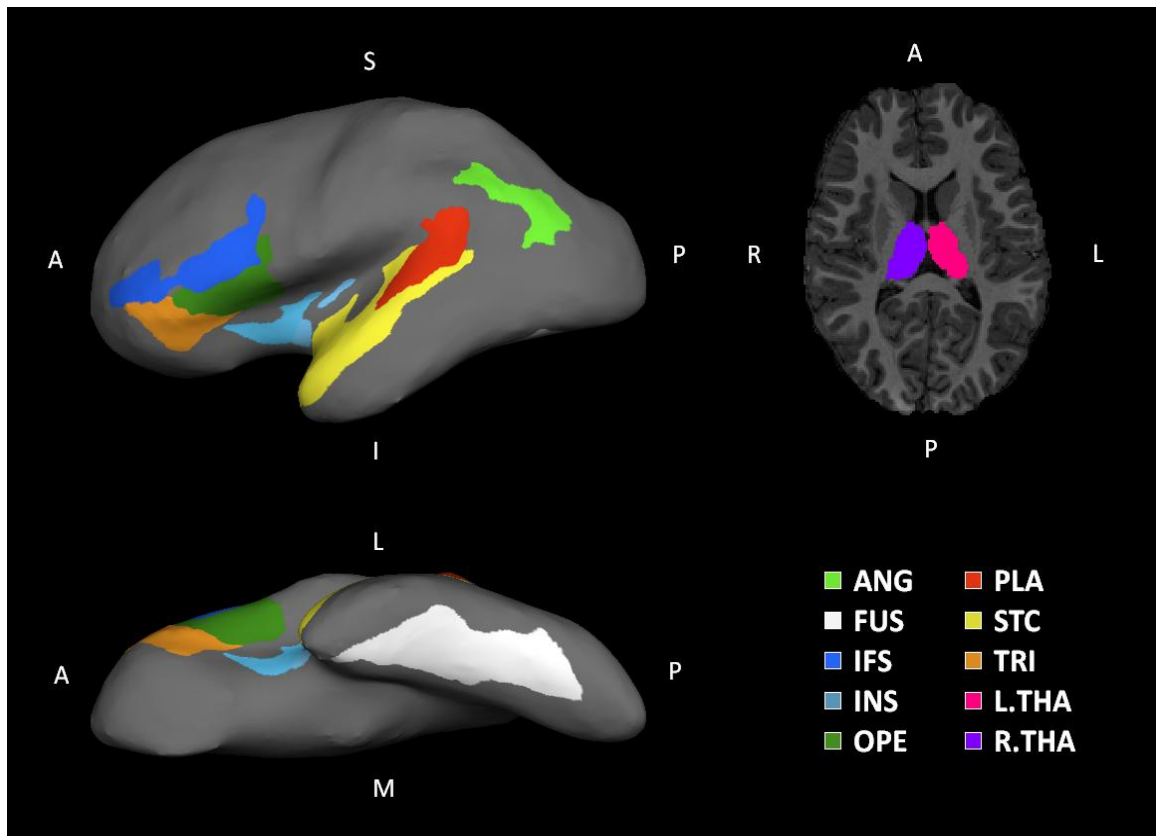


Figure 11. Regions of interest.
Shown in the left column are lateral and inferior views of ROIs rendered on the inflated
surface of a left hemispherical brain. In the right column is a transverse slice of brain
showing THA. 18 ROIs identified in this paper are labeled in the following manner: a
prefix for cerebral hemisphere (L = left hemisphere, R = right hemisphere), a dot
following the prefix, and one of the designators: ANG = Angular Gyrus, FUS =
Fusiform, IFS = Inferior Frontal Sulcus, INS = Insular Cortex, OPE = Pars Opercularis,
PLA = Planum Temporale, STC = Superior Temporal Gyrus, THA = Thalamus, TRI =
Pars Triangularis.

The statistics of regional volumes across participants are shown in Figure 12, with the

cross indicating the mean and the error bar showing standard deviation. The same

anatomical regions on either side of the brain have similar volumes and larger regions

show higher variations across subjects, which is partially due to their bigger surface areas.

Linear regression between regional volumes and behavioral scores was performed, and

no significant correlations were found.
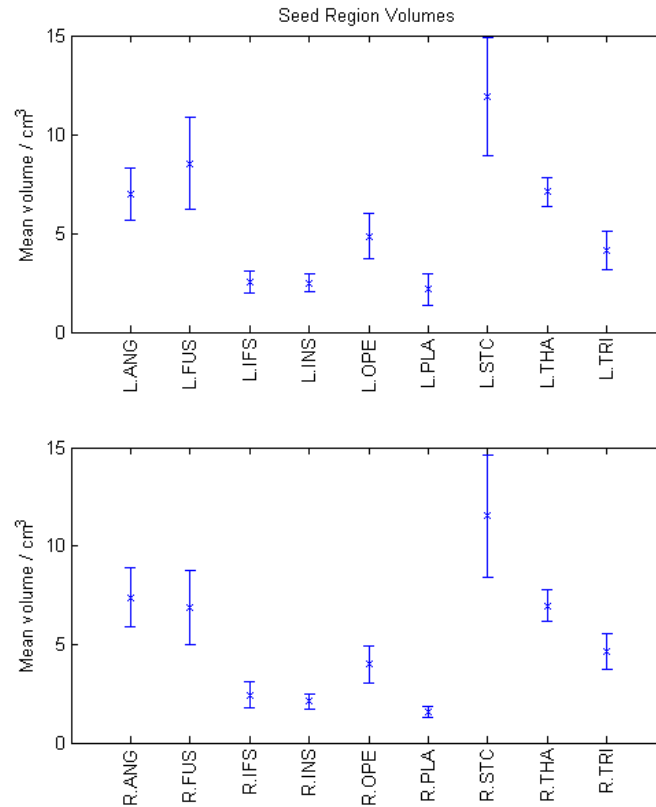


Figure 12. Regional volume statistics.
The regional volumes across subjects are listed, upper panel for the left
hemisphere and lower panel for the right. The same anatomical regions on either
side of the brain have similar volumes. Larger regions show higher variations
across subjects, which is partially due to bigger surface areas. Linear regression
between regional volumes and behavioral scores were performed, and the PDE
subtest of the TOWRE is the only test that correlates with regional volume.

*Local diffusion parameters estimation for probabilistic tractography*

The local diffusion parameters were estimated in FSL using BEDPOSTX. The results are displayed in Figure 13 following Behrens' method (Behrens et al., 2007). In the axial slice (a), the binary mask overlaid on the gray scale FA map shows regions where more than a single fiber orientation was supported by data (thresholded at $f_2 \geq 0.1$ after ARD-based estimation). In the outlined region (b), the mean vectors of the posterior distribution samples on fiber orientations are denoted by short bars, with dominant fiber bundle in red and second in blue. Samples from the posterior distributions on the first two fiber orientations in a voxel (green dot in a, white arrow in b) were displayed on a unit sphere (c) where the lateral motor projections (red) cross the superior longitudinal fasciculus (SLF) projections (blue). The right hand-side is a 90° rotation of the left.
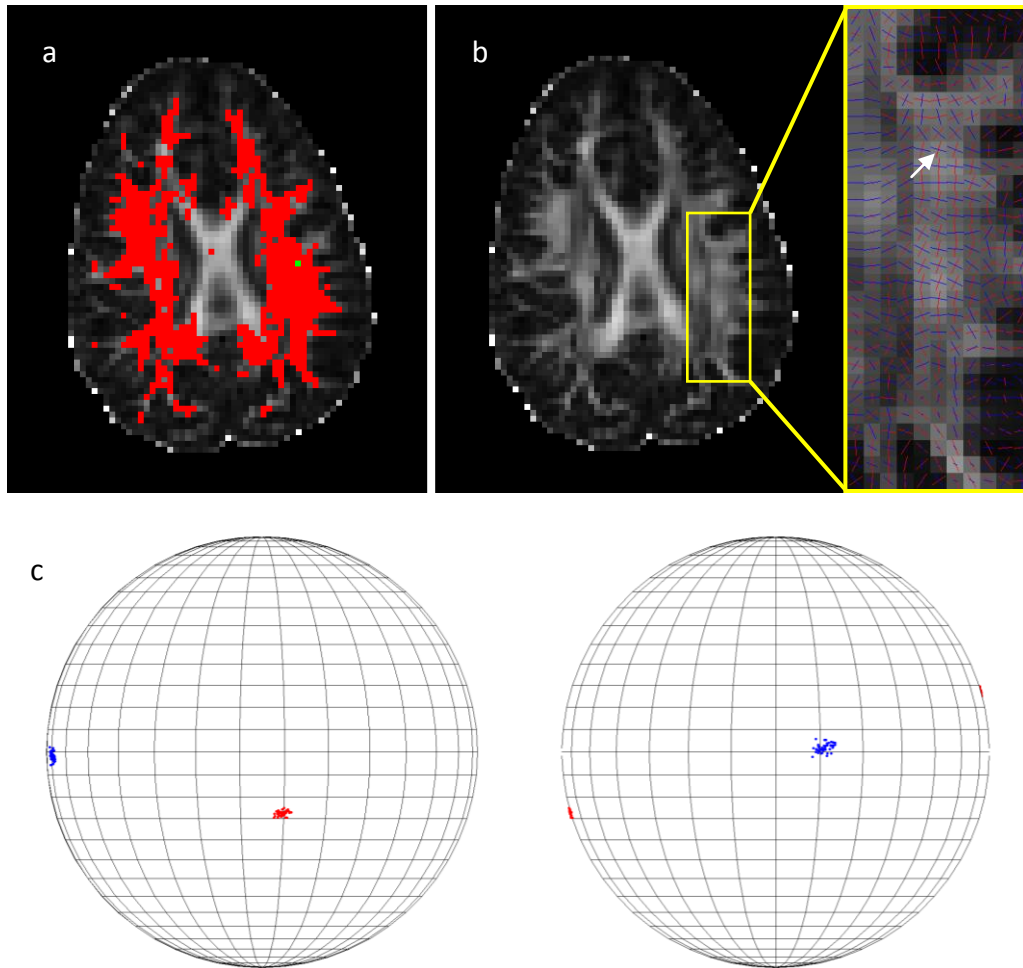
Figure 13. Local diffusion parameters estimation.

In the axial slice (a), the binary mask overlaid on the gray scale FA map shows regions where more than a single fiber orientation was supported by data (thresholded at $f_2 \geq 0.1$ after ARD-based estimation). In the circled region (b), the mean vectors of the posterior distribution samples on fiber orientations are denoted by short bars, with dominant fiber bundle in red and second in blue. Samples from the posterior distributions on the first two fiber orientations in a voxel (green dot in a, white arrow in b) were displayed on a unit sphere (c) where the lateral motor projections (red) cross the superior longitudinal fasciculus (SLF) projections (blue). The right hand-side is a 90° rotation of the left.

*The connectivity matrix*

Connectivity $C_{sym}$ was calculated for each of the possible 72 pairs of regions (within-hemisphere). Figure 14 shows the result of these steps, a connectivity matrix, for one of the control participants in the study. This is a symmetric matrix, with left hemispheric connectivity displayed in the lower left triangle, and right hemispheric in the upper right.
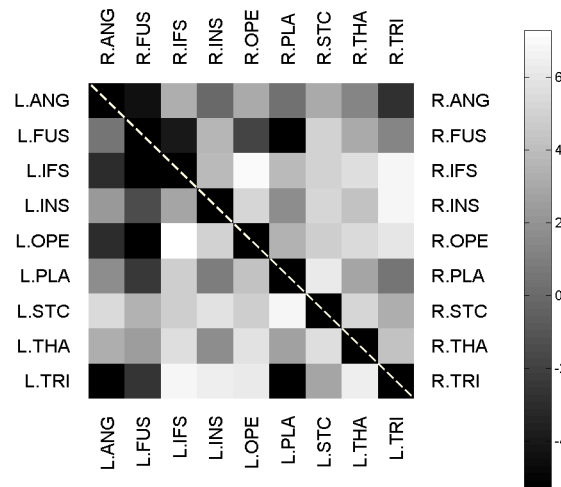


Figure 14. The connectivity matrix.
The matrix of connectivity between all intra-hemispherical pairs of n = 18 ROIs. The pairings within left-hemisphere are displayed in the lower left half, parings within right-hemisphere in the upper right half. All connectivity strengths are displayed with a logarithmic ($\log_{10}$) grayscale map.

## Correlation Analysis

Figure 15 is a visual representation of the correlations between participants' connectivity estimates and their performance on each of the standardized measures. Similar to the connectivity matrices, within the correlation matrices, left hemisphere connections are in the bottom triangle and right hemisphere connections are in the top triangle. The gray scale denotes significance level (p value of correlation analysis, uncorrected for multiple comparisons), with brighter gray indicating more significant correlations. Correlations at the $p < 0.05$ level are identified as significant and labeled with a star. We also investigated age and gender influences on the behavioral and imaging results using two separate one way ANOVAs. Results showed a single significant effect: The left TRI to IFS pathway had a significant gender effect, in which girls had a significantly greater number of white matter fibers connecting these regions. In addition, we correlated participant's performance on the behavioral tasks with the volume of each region. We found a positive correlation between the PDE subtest of the TOWRE and the left planum temporale ($p = .02$) and the left superior temporal cortex ($p = .03$).
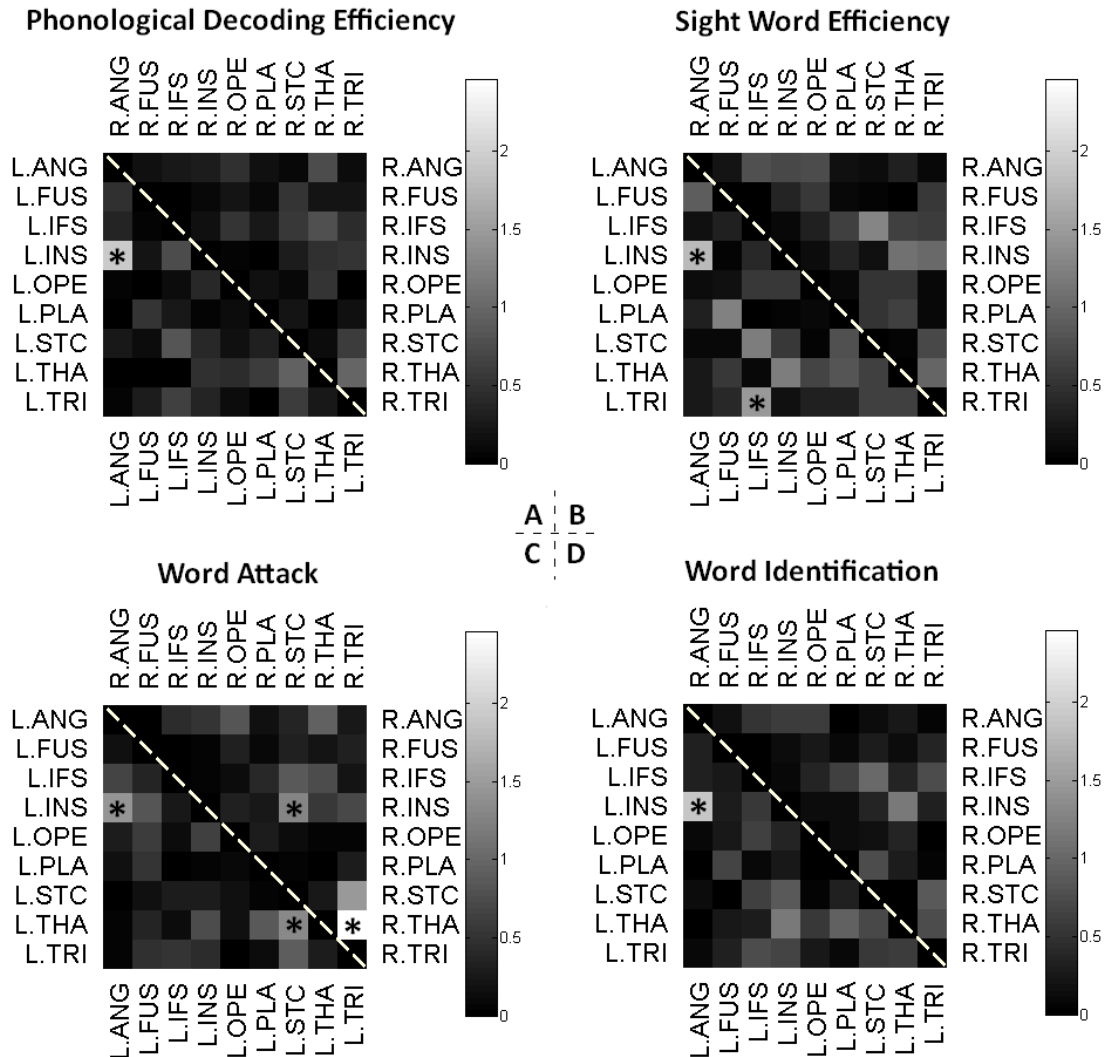
Figure 15. Correlation matrices.
Matrix of correlations between intra-hemispheric pairs of gray matter regions. Connectivity between each pair of ROIs is correlated with Phonological Decoding Efficiency (A), Sight Word Efficiency (B), Word Attack (C), and Word Identification (D), and the significance level of the correlation is displayed on a logarithmic scale. Significant correlations were marked by a star (*p<0.05, uncorrected).

To facilitate interpretation of the significant connections, scatter plots for each finding are shown in Figure 16 and 17. These scatter plots also represent the relationship with response to instruction. In these plots, the NR participants are red, R participants are blue, and CNT participants are green.

# L.ANG and L.INS
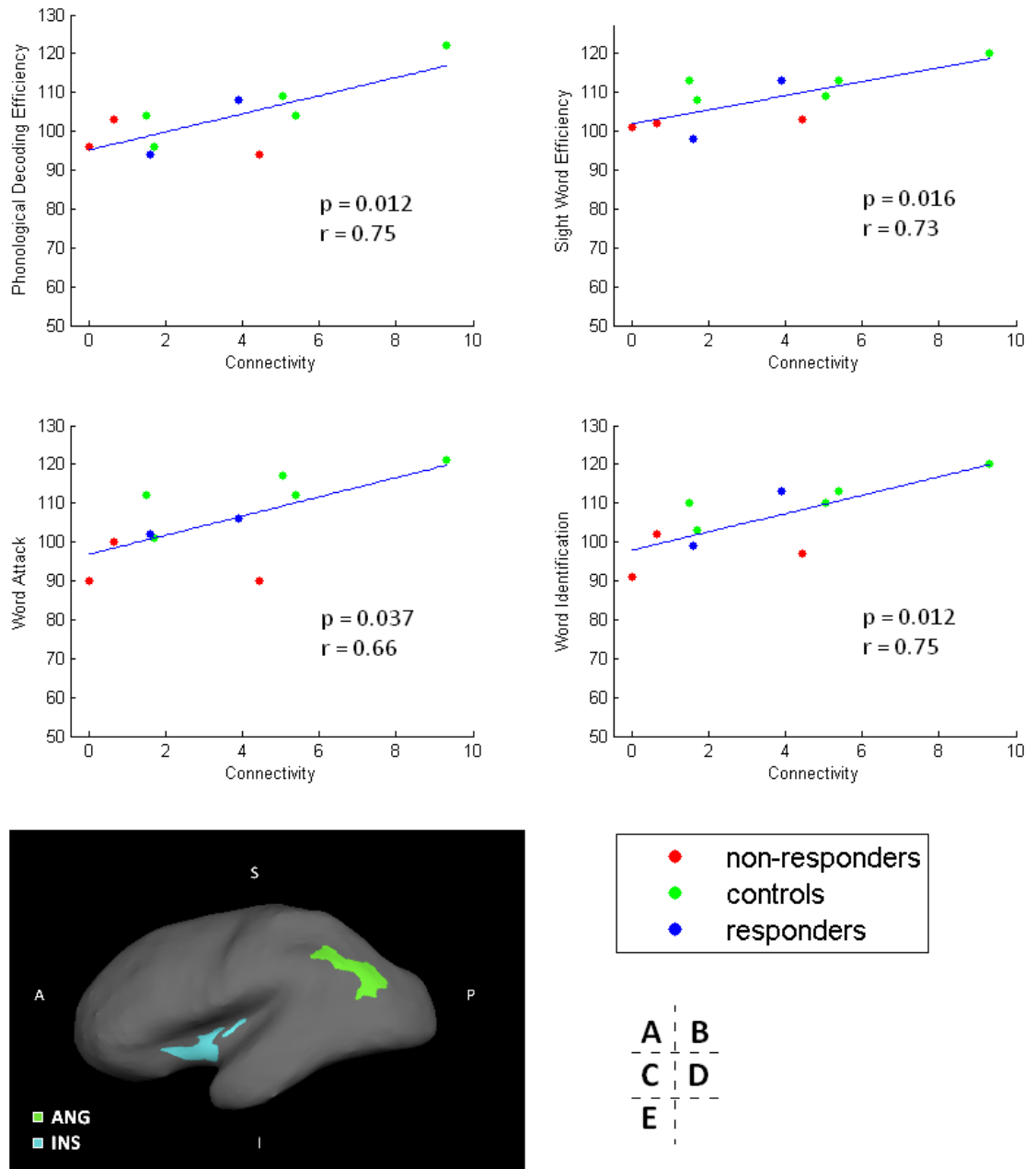


Figure 16. Angular gyrus to insular cortex scatter plots.
Correlation scatter plots for L.INS and L.ANG. (A) - (D) scatter plots showing detailed relationship between connectivity and specific test performance. (E) locations of L.INS and L.ANG. A single NR participant was identified as an outlier and excluded from this analysis.
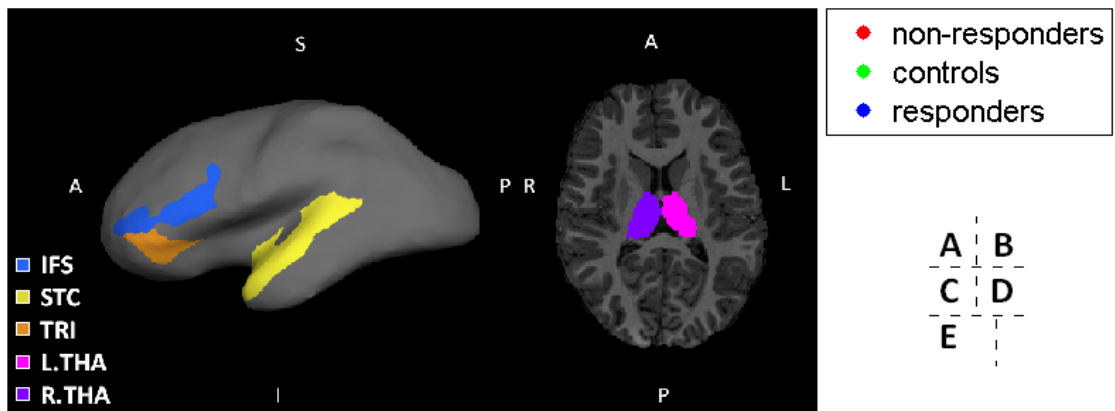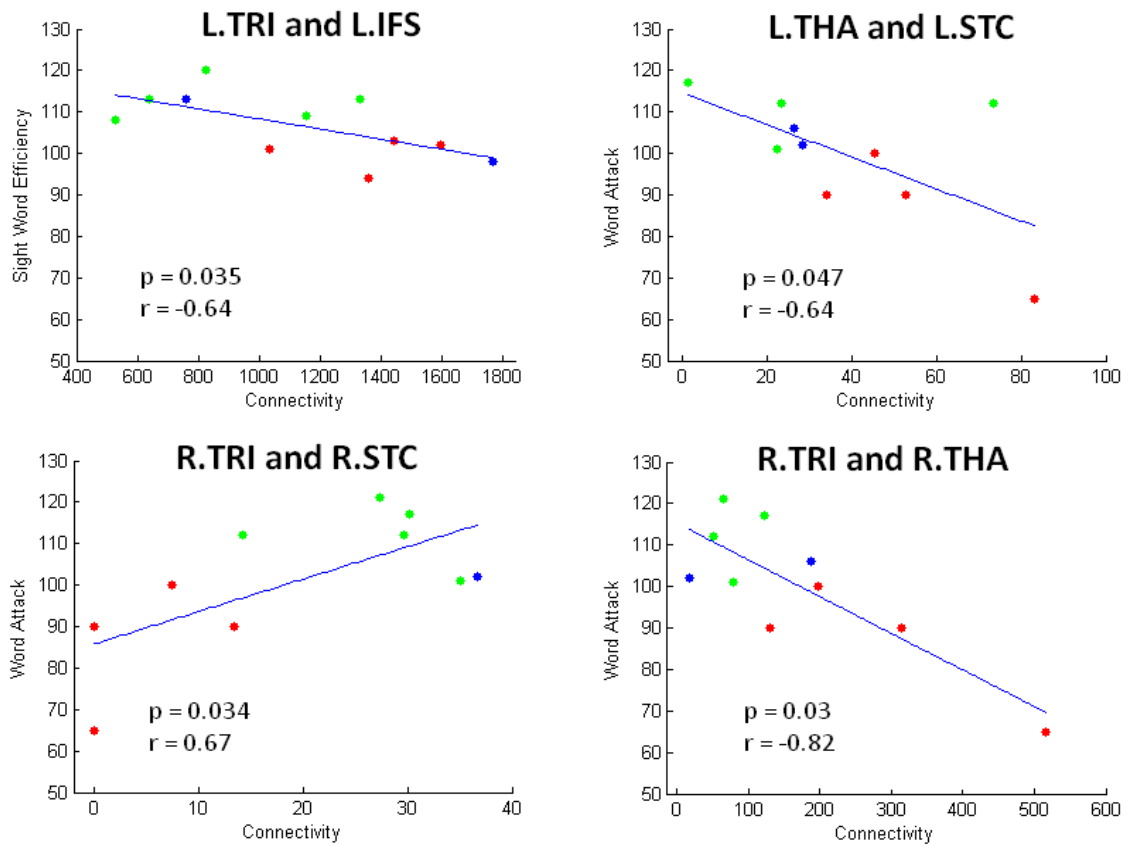
Figure 17. Remaining significant correlations.
Scatter plots showing correlations between connectivity and behavioral test performance. Each scatter plot corresponds to one pair of gray matter regions: (A) L.TRI and L.IFS, (B) L.THA and L.STC, (C) R.STC and R.TRI, (D) R.THA and R.TRI. Locations of these regions are illustrated in (E).

As shown in Figure 16, increased reading score on each of the reading measures is related to greater connectivity between the left ANG and INS; the NR participants generally have lower connectivity than R and CNT participants. Similarly, performance on the WAT subtest correlated positively with connectivity values between TRI to STC (Figure 17). Scatter plots of this correlation showed that NR participants had lower connectivity than R and CNT participants (although only one R dataset survived outlier rejection). Alternatively, three negative correlations were found in which poorer readers, and more particularly, NR participants, had a greater magnitude of connectivity between brain regions than the other two groups. Two correlations involve connections to the THAL, yet in different hemispheres of the brain: the first was right THAL to right TRI and the second was left THAL to left STC. The third remaining region was also in the left hemisphere - TRI to IFS.

CHAPTER IV

DISCUSSION

**Discussion of the Results**

Reading performance requires the involvement of a network of neuronal units that are distributed remotely across the brain. Each neuronal unit has a specific role in modulating brain functions, and only when these units collaborate, can reading behavior be performed. Previous DTI studies have consistently found FA differences between normal readers and poor readers (Beaulieu et al., 2005; Deutsch et al., 2005; Klingberg et al., 2000; Niogi and McCandliss, 2006; Rimrodt et al., 2010), which is suggestive of structural differences in white matter. Given the white matter's role of information transfer, the FA differences, if linked to differences in reading skills, might be a reflection of connectivity variation among individuals. This work is aimed at reconstructing brain connectivity directly and exploring its contribution to reading behaviors via cortico-cortical communication.

Correlation analysis was used to investigate the potential relationship between brain connectivity and reading skills in first graders. The results indicate that eight connectivity estimates correlated with participants' reading skills. Group t-tests were done to show that the correlation was not attributable to differences in gender; we are also confident that the correlation does not arise from age variation. A correlation between brain regional volumes and participants' reading scores was found; however the particular

regions were not involved in the significant connectivity findings. The connectivity results extend the previous findings of white matter differences related to reading skill to identify specific connections between gray matter regions. Furthermore, of the eight significant correlations, four were found in the connections between left angular gyrus and left insular cortex. Regarding the previously reported white matter differences in temporo-pariental regions (Beaulieu et al., 2005; Deutsch et al., 2005; Klingberg et al., 2000; Niogi and McCandliss, 2006; Rimrodt et al., 2010), the results are largely consistent with our findings.

In particular, connectivity between insular cortex and angular gyrus in the left hemisphere correlated with all four reading tasks, indicating that better readers in general had higher connectivity estimates between these two brain regions on both timed and untimed reading tasks. Compared to the other two groups, non-responders had the fewest probabilistic streamlines connecting these two regions. Although the small group sizes limit our statistical power to prove, in a single correlation, the separation of groups with respect to brain connectivity and reading skills, the reoccurrence of the trend across different reading skills is promising.

Nevertheless, interpretation of the findings is challenging, as the insular and the angular gyrus have very different roles. On the one hand, functional activation occurs in the left insular cortex during language, speech, working memory, and attention tasks; in cognition, the left insular cortex also plays an integrative role between purely cognitive and other systems, including sensorimotor, social-emotional, and olfacto-gustatory systems (Chen et al., 2007; Dolan, 2002; Frith and Singer, 2008; Johansen-Berg and Matthews, 2002). On the other hand, the left angular gyrus is important for lexical

processes involved when reading words (Binder et al., 2009), and evidence exists that the angular gyrus is involved in phonological processing, especially at an early age, as inferior parietal lobe is often associated with mapping phonological representations to their orthographic representations (Pugh et al., 2000). These results may indicate that connectivity between these two brain regions is a crucial part of the neural network that supports word recognition skills.

## Discussion of the Methods

Variation in reading skills is due to a combined effect of variations in brain architecture, education, and environment. As age increased, the experience of reading sculpts the brain to form various structural or functional compensations for deficits. Hence, abnormality in children's reading ability as related to brain features is of particular interest, since the gaining of reading experience is just started and the diverse complementary approaches found in the adult population have not been established. This study focuses on brain connectivity in children, and endeavors to identify anatomical features that are characteristic of reading skills.

The employment of probabilistic tractography to estimate the strength of brain connectivity provides the capability to map connections originated from and terminated in gray matter regions directly. In contrast to deterministic tractography, probabilistic tractography is able to trace through locations where the uncertainty in primary diffusion direction estimates is high. On the other hand, due to its high sensitivity to any possible underlying structures, it may give rise to false positive (FP) estimates of streamlines, i.e.,

joining local estimates belonging to different neuronal fiber tracts. Hence, multiple strategies were taken to lower the impact of false positive streamlines on the connectivity estimates, including the utilization of white matter as inclusion masks and cortical regions as termination masks and exclusion masks.

In particular, the thalamus is used as an exclusion mask in all the fiber tracking except for when the tracking is between a region of interest and the thalamus directly. The thalamus is comprised of mixture of white matter and gray matter, and functions as a processing core in the central nervous system. Evidence exists that the thalamus has projections onto the whole cortical surface (Behrens et al., 2003b), and thus any two cortical regions can be connected via the thalamus. However in the scenario of DTI tractography, the tractability of thalamic connections is much higher than that of cortico-cortical connections. For probabilistic fiber tracking algorithms, the number of streamlines detected via the thalamus outweighs the direct cortico-cortical connections, and the analysis will be severely biased towards the thalamic projection distribution consequently. In order to elucidate the contribution of each connection explicitly, the streamlines passing though thalamus are excluded from the statistics. On the other hand, it is possible that the cortico-cortical communication is modulated by the thalamus and the thalamus is indeed believed to be important for reading, so the thalamus is selected as one of the independent regions of interest, and any direct connections between cortical regions and the thalamus is analyzed in the same manner as other cortico-cortical connections (i.e., any relay connections between cortical regions are modeled as two distinct direct connections between the cortical region and the thalamus). Related to this, given the integrative role of the insular cortex, it is highly probable that it serves as a relay station

between nearby neuronal units, but the current study design does not afford the flexibility to keep track of continuing connections explicitly. While the inference is still valid that the direct connections with insular cortex play a key role, interpretation of the role of insular cortex should be made with caution.

This work has several limitations. First of all, a pre-intervention scan was not acquired. Without this information, it is difficult to determine whether the group differences found in this study cause or result from participants' responsiveness to instruction. Future studies would benefit from a longitudinal design, where imaging data are acquired both before and after intervention. Second, at our current level of understanding, it is not possible to determine the causal relationship between gray and white matter deficits. It is possible that fiber pathways are abnormal in reading disability due to a deficit in the number of neurons in one reading-related region projecting along the fiber to other regions. On the other hand, deficits in myelination along a fiber can also impact the efficiency and timing of information transfer between regions, which would cause reductions in activation. A more comprehensive design with functional, structural and diffusion data would be beneficial to study this issue. Third, the regions identified in the current study are parcellated according to anatomically distinguishable landmarks. Some of them are as large as 10 cm$^3$ in volume. Given that many regions are reported to be responsible for multiple cognitive functions in the previous literature, especially for those strip-shaped regions whose anterior tip and posterior tip have different adjacencies, whether the sub-regions bear identical connectivity remains unclear. With refined brain segmentation using anatomical landmarks or smart topological strategies, further exploration of connectivity patterns within each ROI in current study would be fruitful.

Last but not least, due to the limited number of participants in this study, the statistical power available does not allow us to correct for multiple comparisons. A future replication study with an expanded sample size would provide more statistical power and enable more refined analysis of the data.

CHAPTER V


CONCLUSION


This study demonstrates a relationship between brain connectivity and children's reading abilities. Among all the cortical and sub-cortical regions segmented using high resolution structural images, nine regions in each brain hemisphere were selected as important for reading. The probabilistic streamlines connecting each pairing of the nine regions were calculated and used to estimate brain connectivity. The estimates were then used to correlate with children's reading measures.

Eight significant correlations were found, four of which were connections between the insular cortex and angular gyrus. Other correlations involve the connections between the thalamus, triangularis, inferior frontal gyrus and superior temporal cortex. The results are largely consistent with previously reported findings, and are suggestive of a key role of connection between insular cortex and angular gyrus in mediating reading behavior. In spite of the limited sample size, the redundancy in the spread of group clusters among correlation tests is indicative of a relation between brain connectivity and children's responsiveness to intervention.

REFERENCES

Aylward EH, Richards TL, Berninger VW, Nagy WE, Field KM, Grimme AC, Richards AL, Thomson JB, Cramer SC. Instructional treatment associated with changes in brain activation in children with dyslexia. Neurology 2003;61(2):212-219.

Basser PJ, Mattiello J, LeBihan D. MR diffusion tensor spectroscopy and imaging. Biophys J 1994;66(1):259-267.

Basser PJ, Pajevic S, Pierpaoli C, Duda J, Aldroubi A. In vivo fiber tractography using DT-MRI data. Magn Reson Med 2000;44(4):625-632.

Basser PJ, Pierpaoli C. Microstructural and physiological features of tissues elucidated by quantitative-diffusion-tensor MRI. J Magn Reson B 1996;111(3):209-219.

Beaulieu C. The basis of anisotropic water diffusion in the nervous system - a technical review. NMR Biomed 2002;15(7-8):435-455.

Beaulieu C, Allen PS. An in vitro evaluation of the effects of local magnetic-susceptibility-induced gradients on anisotropic water diffusion in nerve. Magn Reson Med 1996;36(1):39-44.

Behrens TE, Berg HJ, Jbabdi S, Rushworth MF, Woolrich MW. Probabilistic diffusion tractography with multiple fibre orientations: What can we gain? Neuroimage 2007;34(1):144-155.

Behrens TE, Johansen-Berg H, Woolrich MW, Smith SM, Wheeler-Kingshott CA, Boulby PA, Barker GJ, Sillery EL, Sheehan K, Ciccarelli O, Thompson AJ, Brady JM, Matthews PM. Non-invasive mapping of connections between human thalamus and cortex using diffusion imaging. Nat Neurosci 2003;6(7):750-757.

Behrens TE, Woolrich MW, Jenkinson M, Johansen-Berg H, Nunes RG, Clare S, Matthews PM, Brady JM, Smith SM. Characterization and propagation of uncertainty in diffusion-weighted MR imaging. Magn Reson Med 2003;50(5):1077-1088.

Binder JR, Desai RH, Graves WW, Conant LL. Where is the semantic system? A critical review and meta-analysis of 120 functional neuroimaging studies. Cereb Cortex 2009;19(12):2767-2796.

Boorman ED, O'Shea J, Sebastian C, Rushworth MF, Johansen-Berg H. Individual differences in white-matter microstructure reflect variation in functional connectivity during choice. Curr Biol 2007;17(16):1426-1431.

Brunswick N, McCrory E, Price CJ, Frith CD, Frith U. Explicit and implicit processing of words and pseudowords by adult developmental dyslexics: A search for Wernicke's Wortschatz? Brain 1999;122 ( Pt 10):1901-1917.

Büchel C, Friston K. Assessing interactions among neuronal systems using functional neuroimaging. Neural Netw 2000;13(8-9):871-882.

Catani M, Jones DK, ffytche DH. Perisylvian language networks of the human brain. Ann Neurol 2005;57(1):8-16.

Chen CH, Ridler K, Suckling J, Williams S, Fu CH, Merlo-Pich E, Bullmore E. Brain imaging correlates of depressive symptom severity and predictors of symptom improvement after antidepressant treatment. Biol Psychiatry 2007;62(5):407-414.

Chen ZJ, He Y, Rosa-Neto P, Germann J, Evans AC. Revealing modular architecture of human brain structural networks by using cortical thickness from MRI. Cereb Cortex 2008;18(10):2374-2381.

Dehaene S, Le Clec'H G, Poline JB, Le Bihan D, Cohen L. The visual word form area: a prelexical representation of visual words in the fusiform gyrus. Neuroreport 2002;13(3):321-325.

Deutsch GK, Dougherty RF, Bammer R, Siok WT, Gabrieli JD, Wandell B. Children's reading performance is correlated with white matter structure measured by diffusion tensor imaging. Cortex 2005;41(3):354-363.

Dolan RJ. Emotion, cognition, and behavior. Science 2002;298(5596):1191-1194.

Fischl B, Liu A, Dale AM. Automated manifold surgery: constructing geometrically accurate and topologically correct models of the human cerebral cortex. IEEE Trans Med Imaging 2001;20(1):70-80.

Fischl B, Salat DH, Busa E, Albert M, Dieterich M, Haselgrove C, van der Kouwe A, Killiany R, Kennedy D, Klaveness S, Montillo A, Makris N, Rosen B, Dale AM. Whole brain segmentation: automated labeling of neuroanatomical structures in the human brain. Neuron 2002;33(3):341-355.

Fischl B, Salat DH, van der Kouwe AJ, Makris N, Ségonne F, Quinn BT, Dale AM. Sequence-independent segmentation of magnetic resonance images. Neuroimage 2004;23 Suppl 1:S69-84.

Friston KJ, Frith CD, Liddle PF, Frackowiak RS. Functional connectivity: the principal-component analysis of large (PET) data sets. J Cereb Blood Flow Metab 1993;13(1):5-14.

Friston KJ. Functional and effective connectivity in neuroimaging: a synthesis. Hum Brain Mapp 1994;2(1):56–78.

Frith CD, Singer T. The role of social cognition in decision making. Philos Trans R Soc Lond B Biol Sci 2008;363(1511):3875-3886.

Hagmann P, Cammoun L, Gigandet X, Meuli R, Honey CJ, Wedeen VJ, Sporns O. Mapping the structural core of human cerebral cortex. PLoS Biol 2008;6(7):e159.

Hagmann P, Kurant M, Gigandet X, Thiran P, Wedeen VJ, Meuli R, Thiran JP. Mapping human whole-brain structural networks with diffusion MRI. PLoS One 2007;2(7):e597.

He Y, Chen ZJ, Evans AC. Small-world anatomical networks in the human brain revealed by cortical thickness from MRI. Cereb Cortex 2007;17(10):2407-2419.

Honey CJ, Kötter R, Breakspear M, Sporns O. Network structure of cerebral cortex shapes functional connectivity on multiple time scales. Proc Natl Acad Sci U S A 2007;104(24):10240-10245.

Horwitz B, Rumsey JM, Donohue BC. Functional connectivity of the angular gyrus in normal reading and dyslexia. Proc Natl Acad Sci U S A 1998;95(15):8939-8944.

IDEA, Public Law 108–446 2004;118 STAT. 2647, 2657–2658.

Jenkinson M. Fast, automated, N-dimensional phase-unwrapping algorithm. Magn Reson Med 2003;49(1):193-197.

Jenkinson M, Smith S. A global optimisation method for robust affine registration of brain images. Med Image Anal 2001;5(2):143-156.

Jenkinson M. Improved Unwarping of EPI Volumes using Regularised B0 Maps. In Seventh Annual Meeting of the Organization for Human Brain Mapping - HBM. 2001.

Jenkinson M. Improving the Registration of B0-distorted EPI Images using Calculated Cost Function Weights. In Tenth Annual Meeting of the Organization for Human Brain Mapping - HBM. 2004

Jezzard P, Balaban RS. Correction for geometric distortion in echo planar images from B0 field variations. Magn Reson Med 1995;34(1):65-73.

Johansen-Berg H, Behrens TE, Robson MD, Drobnjak I, Rushworth MF, Brady JM, Smith SM, Higham DJ, Matthews PM. Changes in connectivity profiles define functionally distinct regions in human medial frontal cortex. Proc Natl Acad Sci U S A 2004;101(36):13335-13340.

Johansen-Berg H, Matthews PM. Attention to movement modulates activity in sensori-motor areas, including primary motor cortex. Exp Brain Res 2002;142(1):13-24.

Johnston JM, Vaishnavi SN, Smyth MD, Zhang D, He BJ, Zempel JM, Shimony JS, Snyder AZ, Raichle ME. Loss of resting interhemispheric functional connectivity after complete section of the corpus callosum. J Neurosci 2008;28(25):6453-6458.

Jones DK. Determining and visualizing uncertainty in estimates of fiber orientation from diffusion tensor MRI. Magn Reson Med 2003;49(1):7-12.

Jones DK. Tractography gone wild: probabilistic fibre tracking using the wild bootstrap with diffusion tensor MRI. IEEE Trans Med Imaging 2008;27(9):1268-1274.

Klingberg T, Hedehus M, Temple E, Salz T, Gabrieli JD, Moseley ME, Poldrack RA. Microstructure of temporo-parietal white matter as a basis for reading ability: evidence from diffusion tensor magnetic resonance imaging. Neuron 2000;25(2):493-500.

Lazar M, Alexander AL. An error analysis of white matter tractography methods: synthetic diffusion tensor field simulations. Neuroimage 2003;20(2):1140-1153.

Lori NF, Akbudak E, Shimony JS, Cull TS, Snyder AZ, Guillory RK, Conturo TE. Diffusion tensor fiber tracking of human brain connectivity: aquisition methods, reliability analysis and biological results. NMR Biomed 2002;15(7-8):494-515.

Mesulam MM. Large-scale neurocognitive networks and distributed processing for attention, language, and memory. Ann Neurol 1990;28(5):597-613.

Mori S, Crain BJ, Chacko VP, van Zijl PC. Three-dimensional tracking of axonal projections in the brain by magnetic resonance imaging. Ann Neurol 1999;45(2):265-269.

Mori S, van Zijl PC. Fiber tracking: principles and strategies - a technical review. NMR Biomed 2002;15(7-8):468-480.

Moseley ME, Cohen Y, Kucharczyk J, Mintorovitch J, Asgari HS, Wendland MF, Tsuruda J, Norman D. Diffusion-weighted MR imaging of anisotropic water diffusion in cat central nervous system. Radiology 1990;176(2):439-445.

Netsch T, van Muiswinkel A. Quantitative evaluation of image-based distortion correction in diffusion tensor imaging. IEEE Trans Med Imaging 2004;23(7):789-798.

Niogi SN, McCandliss BD. Left lateralized white matter microstructure accounts for individual differences in reading ability and disability. Neuropsychologia 2006;44(11):2178-2188.

Nittrouer S. Do temporal processing deficits cause phonological processing problems? J Speech Lang Hear Res 1999;42(4):925-942.

Pajevic S, Aldroubi A, Basser PJ. A continuous tensor field approximation of discrete DT-MRI data for extracting microstructural and architectural features of tissue. J Magn Reson 2002;154(1):85-100.

Parker GJ, Alexander DC. Probabilistic Monte Carlo based mapping of cerebral connections utilising whole-brain crossing fibre information. Inf Process Med Imaging 2003;18:684-695.

Parker GJ, Alexander DC. Probabilistic anatomical connectivity derived from the microscopic persistent angular structure of cerebral tissue. Philos Trans R Soc Lond B Biol Sci 2005;360(1457):893-902.

Paulesu E, Démonet JF, Fazio F, McCrory E, Chanoine V, Brunswick N, Cappa SF, Cossu G, Habib M, Frith CD, Frith U. Dyslexia: cultural diversity and biological unity. Science 2001;291(5511):2165-2167.

Perry C, Ziegler JC, Zorzi M. Nested incremental modeling in the development of computational theories: the CDP+ model of reading aloud. Psychol Rev 2007;114(2):273-315.

Pierpaoli C, Basser PJ. Toward a quantitative assessment of diffusion anisotropy. Magn Reson Med 1996;36(6):893-906.

Puce A, Allison T, Asgari M, Gore JC, McCarthy G. Differential sensitivity of human visual cortex to faces, letterstrings, and textures: a functional magnetic resonance imaging study. J Neurosci 1996;16(16):5205-5215.

Pugh KR, Mencl WE, Shaywitz BA, Shaywitz SE, Fulbright RK, Constable RT, Skudlarski P, Marchione KE, Jenner AR, Fletcher JM, Liberman AM, Shankweiler DP, Katz L, Lacadie C, Gore JC. The angular gyrus in developmental dyslexia: task-specific differences in functional connectivity within posterior cortex. Psychol Sci 2000;11(1):51-56.

Rimrodt SL, Peterson DJ, Denckla MB, Kaufmann WE, Cutting LE. White matter microstructural differences linked to left perisylvian language network in children with dyslexia. Cortex 2010;46(6):739-749.

Rumsey JM, Horwitz B, Donohue BC, Nace K, Maisog JM, Andreason P. Phonological and orthographic components of word recognition. A PET-rCBF study. Brain 1997;120 ( Pt 5):739-759.

Rykhlevskaia E, Gratton G, Fabiani M. Combining structural and functional neuroimaging data for studying brain connectivity: a review. Psychophysiology 2008;45(2):173-187.

Ségonne F, Dale AM, Busa E, Glessner M, Salat D, Hahn HK, Fischl B. A hybrid approach to the skull stripping problem in MRI. Neuroimage 2004;22(3):1060-1075.

Ségonne F, Pacheco J, Fischl B. Geometrically accurate topology-correction of cortical surfaces using nonseparating loops. IEEE Trans Med Imaging 2007;26(4):518-529.

Shaywitz BA, Shaywitz SE, Blachman BA, Pugh KR, Fulbright RK, Skudlarski P, Mencl WE, Constable RT, Holahan JM, Marchione KE, Fletcher JM, Lyon GR, Gore JC. Development of left occipitotemporal systems for skilled reading in children after a phonologically- based intervention. Biol Psychiatry 2004;55(9):926-933.

Shaywitz SE, Shaywitz BA. Dyslexia (specific reading disability). Pediatr Rev 2003;24(5):147-153.

Simos PG, Fletcher JM, Bergman E, Breier JI, Foorman BR, Castillo EM, Davis RN, Fitzgerald M, Papanicolaou AC. Dyslexia-specific brain activation profile becomes normal following successful remedial training. Neurology 2002;58(8):1203-1213.

Simos PG, Fletcher JM, Denton C, Sarkari S, Billingsley-Marshall R, Papanicolaou AC. Magnetic source imaging studies of dyslexia interventions. Dev Neuropsychol 2006;30(1):591-611.

Sled JG, Zijdenbos AP, Evans AC. A nonparametric method for automatic correction of intensity nonuniformity in MRI data. IEEE Trans Med Imaging 1998;17(1):87-97.

Smith SM, Jenkinson M, Woolrich MW, Beckmann CF, Behrens TE, Johansen-Berg H, Bannister PR, De Luca M, Drobnjak I, Flitney DE, Niazy RK, Saunders J, Vickers J, Zhang Y, De Stefano N, Brady JM, Matthews PM. Advances in functional and structural MR image analysis and implementation as FSL. Neuroimage 2004;23 Suppl 1:S208-219.

Sporns O, Honey CJ, Kötter R. Identification and classification of hubs in brain networks. PLoS One 2007;2(10):e1049.

Stejskal EO, Tanner JE. Spin Diffusion Measurements: Spin Echoes in the Presence of a Time-Dependent Field Gradient. J Chem Phys 1965;42(1):288-292.

Tarkiainen A, Cornelissen PL, Salmelin R. Dynamics of visual feature analysis and object-level processing in face versus letter-string perception. Brain 2002;125(Pt 5):1125-1136.

Temple E, Poldrack RA, Salidis J, Deutsch GK, Tallal P, Merzenich MM, Gabrieli JD. Disrupted neural responses to phonological and orthographic processing in dyslexic children: an fMRI study. Neuroreport 2001;12(2):299-307.

Whitcher B, Tuch DS, Wisco JJ, Sorensen AG, Wang L. Using the wild bootstrap to quantify uncertainty in diffusion tensor imaging. Hum Brain Mapp 2008;29(3):346-362.

Woolrich MW, Jbabdi S, Patenaude B, Chappell M, Makni S, Behrens T, Beckmann C, Jenkinson M, Smith SM. Bayesian analysis of neuroimaging data in FSL. Neuroimage 2009;45(1 Suppl):S173-186.